

FACULDADE DE ENGENHARIA DA UNIVERSIDADE DO PORTO



Energy Optimization in Railway Systems

André Duarte da Fonseca

Mestrado Integrado em Engenharia Eletrotécnica e de Computadores

Supervisor: Adriano da Silva Carvalho

July 29, 2021

Resumo

O transporte ferroviário de alta velocidade é o meio de transporte energeticamente mais eficiente e amigo do ambiente, mas apesar disso, aumentar a eficiência deste transporte em apenas alguns pontos percentuais pode levar a grandes poupanças a nível económico e ambiental.

Há vários anos que a utilização de sistemas adicionais que permitam aumentar a eficiência dos transportes ferroviários tem vindo a ser discutida mas, até agora, a implementação destes sistemas ainda é bastante baixa. Estes sistemas podem ser para gerar energia e reduzir as necessidades da rede ou para regenerar energia que atualmente é desperdiçada e dissipada sobre a forma de calor.

Para a geração de energia, esta dissertação propõe a implementação de um sistema de geração fotovoltaico que gera energia elétrica através da luz solar. Como os comboios viajam maioritariamente à superfície e em zonas livres de vegetação, este sistema tem a possibilidade de ter um impacto significativo na energia que é consumida pelos sistemas auxiliares do comboio.

No que respeita o sistema de recuperação de energia, esta dissertação propõe a implementação de um sistema de armazenamento de energia a bordo do comboio, que seja capaz de armazenar a energia gerada a partir da funcionalidade de travagem elétrica disponível no comboio. Esta energia pode depois ser utilizada em períodos com necessidades de energia superiores de modo a reduzir o pico de potência do sistema total.

Ambos os sistemas requerem a implementação de conversores de potência bem como de controladores para os gerirem. Após a criação de um modelo do sistema elétrico atual do comboio, a implementação destes conversores e dos respetivos controladores será o foco desta dissertação.

Palavras-chave: Ferrovia, Eficiência Energética, Energia Solar, Sistemas de Armazenamento de Energia A bordo

Abstract

High speed rail transportation is the most energy efficient and environmentally friendly way to travel, but even so, improving these transports efficiency by just a few percentage points can lead to major economical and environmental savings.

For some years the use of additional systems that increase the railway's efficiency have been discussed but, so far, their implementation is still very scarce. Such systems can be either to generate power to reduce the grid requirements or to regenerate power that is currently being wasted and dissipated as heat.

For the power generation, in this dissertation it is proposed the implementation of a photo-voltaic system that generates electrical power from the sun light. Since the trains mostly travel on above ground rails in areas clear of vegetation, this system has the possibility to have a significant impact in the power that is consumed by the auxiliary systems of the train.

Regarding the energy recovery system, this dissertation proposes the implementation of an onboard energy storage system that is capable of storing the energy generated from the electrical braking capability of the train. This energy can then be used during periods with higher energy needs in order to reduce the peak power of the overall system.

Both these systems require power converters to be implemented along with some controllers to manage them. After creating a model of the current electrical system of the train, the implementation of these converters and controllers will be the focus of this dissertation.

Keywords: Railway, Energy Efficiency, Solar Energy, OESS

Agradecimentos

Quero agradecer à Faculdade de Engenharia e ao Professor Doutor Adriano da Silva Carvalho pela oportunidade de realizar esta dissertação e pelo apoio prestado ao longo da mesma.

Quero agradecer também a todos os meus familiares por todo o apoio que me deram ao longo de todos os anos de percurso escolar, em particular aos meus tios João e Felicidade Duarte pois sem a sua ajuda não teria entrado para esta faculdade.

A todos os meus colegas e amigos com quem partilhei muitos momentos de trabalho e diversão ao longo dos últimos cinco anos.

E em especial aos meus pais, António Fonseca e Fernanda Duarte, pelo apoio incondicional que me deram durante vinte e três anos e sem o seu esforço e trabalho certamente não estaria aqui hoje.

André Fonseca

*“Think of how stupid the average person is,
and realize half of them are stupider than that.”*

George Carlin

Contents

1	Introduction	1
1.1	Context and Motivation	1
1.2	Objectives	1
1.3	Document Structure	2
2	State of the Art	3
2.1	Introduction	3
2.2	Clarke and Park transforms	3
2.2.1	Clarke Transform	3
2.2.2	Park Transform	4
2.3	Induction Motor	5
2.4	Energy Storage System	6
2.5	Regenerative Breaking	8
2.5.1	High Voltage ESS	9
2.5.2	Low Voltage ESS	9
2.5.3	Charging Control	10
2.6	Photovoltaic Panels	10
3	Simulation Model	13
3.1	Summary	13
3.2	Physical Model	13
3.2.1	Resistive Forces	13
3.2.2	Traction Force	17
3.2.3	Train Movement	19
3.2.4	Matlab Implementation	23
3.3	Micro Grid	23
3.4	Traction System	24
3.4.1	AC/DC Converter	24
3.4.2	AC/DC Converter Controller	26
3.4.3	DC/AC Inverter	27
3.4.4	DC/AC Inverter and Motor Control	29
3.5	Auxiliary Systems	37
3.6	Conclusions	39
4	Photovoltaic Production System	41
4.1	Summary	41
4.2	Array Configurations	41
4.3	DC/DC converter	43

4.4	DC/DC converter controller (MPPT)	46
5	Energy Storage System	49
5.1	Summary	49
5.2	Comparison	49
5.3	Matlab implementation	51
5.4	DC/DC converter	51
5.5	DC/DC converter control	52
5.5.1	Charging OESS	52
5.5.2	Discharging OESS	53
6	Results	55
6.1	Photovoltaic Production System	55
6.2	Onboard Energy Storage System	60
7	Conclusion	65
7.1	Final Remarks	65
7.2	Future Work	65
A	C Code	67
A.1	Code used to calculate the acceleration time of the train	67
A.2	Code used to calculate the deceleration time of the train	68
B	Traction System	69
B.1	Torque Reference Controller	70
B.2	Electrical System	71
C	Schematic	73
C.1	Series 4000 schematic	74
D	MPPT	75
D.1	MPPT implementation	76
	References	77

List of Figures

2.1	High voltage ESS bidirectional Charging/Discharging converter[1]	9
2.2	Low voltage ESS bidirectional Charging/Discharging converter [1]	10
3.1	Resistive Forces across the operating speed range	15
3.2	Traction Force across the operating speed range	18
3.3	Matlab/Simulink implementation of the train's physical model	23
3.4	Train's micro grid general structure	24
3.5	AC/DC power converter for the traction system	25
3.6	AC/DC converter controller implementation in Matlab/Simulink	26
3.7	DC/AC Inverter powering 3 phase induction motor	27
3.8	Simulink block used to calculate the power factor of the motor	28
3.9	Implemented FOC controller block diagram	29
3.10	Implemented Flux Reference Controller	30
3.11	Implemented d axis controller	31
3.12	Operation mode Selector state machine	32
3.13	Acceleration sub-controller	33
3.14	Cruising sub-controller	34
3.15	Cruising torque reference compensation PI controller	34
3.16	Maximum torque reference offset controller	35
3.17	Implemented q axis controller	36
3.18	SVPWM motor controller Matlab/Simulink implementation	36
3.19	Torque and Flux estimator implementation in Matlab/Simulink	37
3.20	AC/DC power converter for the auxiliary systems	38
3.21	DC/AC inverter grid forming controller implementation in Matlab/Simulink	38
3.22	Electrical model of the traction system implemented in Matlab/Simulink	39
4.1	Cross section of a carriage from a series 4000 train [2]	42
4.2	DC/DC Boost converter structure	44
4.3	Solar panel I-V characteristic curve (top), Solar panel P-V characteristic curve (bottom)	45
4.4	DC/DC Boost converter and solar array implementation in Matlab/Simulink	45
4.5	MPPT Perturb and Observe diagram	46
5.1	DC/DC bidirectional converter charge controller	52
5.2	DC/DC bidirectional converter discharge controller	53
6.1	Current consumed by the auxiliary systems without photovoltaic system connected	55
6.2	Current consumed by the auxiliary systems with photovoltaic system connected with nominal irradiance	56

6.3	Voltage at the output of an array of 90 solar panels	56
6.4	Current at the output of an array of 90 solar panels	57
6.5	Power outputted by an array of 90 solar panels	57
6.6	Current consumed by the auxiliary systems with photovoltaic system connected with an irradiance variation from 1000 to 750 W/m ²	58
6.7	Voltage at the output of an array of 90 solar panels with an irradiance variation from 1000 to 750 W/m ²	58
6.8	Current at the output of an array of 90 solar panels with an irradiance variation from 1000 to 750 W/m ²	59
6.9	Power outputted by an array of 90 solar panels with an irradiance variation from 1000 to 750 W/m ²	59
6.10	Velocity of the train during acceleration and deceleration test without OESS	60
6.11	Torque of one of the motors of the train during acceleration and deceleration test without OESS	61
6.12	Charge consumed from the catenary by the traction system of the train during acceleration and deceleration test without OESS	61
6.13	Velocity of the train during acceleration and deceleration test with OESS	62
6.14	Torque of one of the motors of the train during acceleration and deceleration test with OESS	63
6.15	Charge consumed from the catenary by the traction system of the train during acceleration and deceleration test with OESS	63
6.16	Voltage of the capacitor bank of the train during acceleration and deceleration test with OESS	64
A.1	Code used to calculate the acceleration time of the train	67
A.2	Code used to calculate the deceleration time of the train	68
B.1	Torque Reference Controller implementation in Matlab/Simulink	70
B.2	Electrical model of the traction system implemented in Matlab/Simulink	71
C.1	Schematic of the series 4000 train from [3]	74
D.1	MPPT algorithm implementation in Matlab/Simulink	76

List of Tables

2.1	Energy density, cycle life and operating temperature of batteries [4]	7
3.1	Calculated acceleration times from standstill to top speed with multiple step sizes	21
3.2	Calculated deceleration times from top speed to a standstill with multiple step sizes	22
3.3	Three phase induction motor parameters	28
4.1	Number of panels and installed power for each type of carriage	43
4.2	Solar panel characteristics	43
4.3	DC voltage of the panel strings for each carriage type	43
4.4	Duty-cycles of the DC/DC boost converters for each carriage type	44

Abbreviations and Symbols

ESS	Energy Storage System
OESS	Onboard Energy Storage System
Li-Ion	Lithium-Ion
Li-Polymer	Lithium Polymer
Ni-Mh	Nickel–metal hydride
Ni-Cd	Nickel–cadmium
Ni-Zn	Nickel–zinc
DC	Direct Current
DC/DC	Direct Current to Direct Current
AC	Alternating Current
AC/AC	Alternating Current to Alternating Current
AC/DC	Alternating Current to Direct Current
DC/AC	Direct Current to Alternating Current
MPPT	Maximum Power Point Tracker
RMS	Root Mean Square
PWM	Pulse Width Modulation
SVPWM	Space Vector Pulse Width Modulation
FOC	Field Oriented Control
PI	Proportional Integral
IM	Induction Motor

Chapter 1

Introduction

1.1 Context and Motivation

In the 18th century, with the advent of the steam engine, rail transportation played a key role in the industrial revolution by allowing large numbers of people and goods to be transported over long distances.

In the 21st century, energy efficiency has become the main focus of transportation. Being the mode of transport with the lowest impact on the environment, high speed rail transportation can significantly lower the CO₂ emissions of the transportation sector, which constitutes 24% of the global emissions [5]. Due to the current context of climatic emergency, high-speed rail transportation could be as important today, as the steam locomotives were in the 18th century.

Despite being the most energy efficient way to move, the continuous evolution of technological solutions leaves room for significant improvement in this context. The high fluctuations in the power requirements from a railway system is currently their main problem. Power spikes lead to high losses and contribute to the overall instability of whole the electrical grid.

The pressure and incentives imposed by the European Union towards the decarbonization of the economy paves the way for major investment in sustainable forms of transportation, which, in turn, opens the possibility for new technologies to be developed and implemented.

1.2 Objectives

On the course of this project it is intended to develop a system that solves some of the major problems that face railway systems. This approach will focus mainly on the development of two complementary systems for the high speed trains currently used in the "Linha do Norte" railway system. These systems consist of a renewable energy production, and a storage system for the regenerative braking system. Together it is expected that all systems will provide a significant reduction on both the average and the maximum power requested by the the train electrical system to the grid, providing not only a positive environmental impact but also a cost reduction to the system operator.

1.3 Document Structure

Besides the introduction, there are five more chapters in this dissertation. In the second chapter, the state of the art is presented with the concepts that are considered most important for the development of the work of this dissertation.

The third chapter focuses on the development of the simulation model implemented in the simulation software Matlab/Simulink. The modeling of the train's system goes from defining its physical model to the implementation of all the required electrical converters to their respective controllers.

In the fourth chapter the photovoltaic production system is characterized and its implementation is explained including the power converter and its respective controller.

The fifth chapter refers to the on board energy storage system and begin with the sizing and comparison of two possible solutions for this system. Then the bidirectional converter is presented along with the charge and discharge controllers.

Chapter six presents the power saving and peak shaving results obtained from the implemented systems.

To finalize, chapter seven presents the global conclusions of this dissertation along with the future work that can be built over the work developed in this dissertation.

Chapter 2

State of the Art

2.1 Introduction

In order to decide the best approach to the problem previously described, the currently available literature was analysed and different solutions have been compared. This chapter will begin by presenting the principles of the dq reference frame and the working principles of an induction motor, followed by the analysis of the energy storage system and the regenerative braking system and to finish this bibliographic review the photovoltaic generation system will be analysed.

2.2 Clarke and Park transforms

Currently the control of any kind of electric motor is reliant on the principles of the Clarke and Park mathematical transforms.

For a balanced three phase current system, as an induction motor, the current i_a , i_b and i_c can be written as the equations that follow, where I is the RMS value of the currents.

$$i_a(t) = \sqrt{2} \cdot I \cdot \cos(\theta(t)) \quad (2.1)$$

$$i_b(t) = \sqrt{2} \cdot I \cdot \cos\left(\theta(t) + \frac{\pi}{3}\right) \quad (2.2)$$

$$i_c(t) = \sqrt{2} \cdot I \cdot \cos\left(\theta(t) + \frac{2\pi}{3}\right) \quad (2.3)$$

2.2.1 Clarke Transform

The Clarke transform takes a three phase AC electrical system (like an induction motor), and converts it into a two phase system. This transformation simplifies the circuit and allows the

control to be done with just two variables instead of three. This transform is implemented as follows [6]:

$$i_{\alpha\beta 0}(t) = \frac{2}{3} \cdot \begin{bmatrix} 1 & -\frac{1}{2} & -\frac{1}{2} \\ 0 & \frac{\sqrt{3}}{2} & -\frac{\sqrt{3}}{2} \\ \frac{1}{2} & \frac{1}{2} & \frac{1}{2} \end{bmatrix} \cdot \begin{bmatrix} i_a(t) \\ i_b(t) \\ i_c(t) \end{bmatrix} \quad (2.4)$$

From the Clarke transform, the $i_{\alpha\beta 0}$ currents can be written by the mathematical expressions below.

$$i_{\alpha}(t) = \sqrt{2} \cdot I \cdot \cos(\theta(t)) \quad (2.5)$$

$$i_{\beta}(t) = \sqrt{2} \cdot I \cdot \sin(\theta(t)) \quad (2.6)$$

$$i_0(t) = 0 \quad (2.7)$$

After being processed by a controller there can be the necessity to reverse this conversion, transforming $i_{\alpha\beta 0}$ back into i_a , i_b and i_c . This is done with the inverse Clarke's transform by means of the matrix presented in equation 2.8.

$$i_{abc}(t) = \begin{bmatrix} 1 & 0 & 1 \\ -\frac{1}{2} & \frac{\sqrt{3}}{2} & 1 \\ -\frac{1}{2} & -\frac{\sqrt{3}}{2} & 1 \end{bmatrix} \cdot \begin{bmatrix} i_{\alpha}(t) \\ i_{\beta}(t) \\ i_0(t) \end{bmatrix} \quad (2.8)$$

2.2.2 Park Transform

The outputs of the Clarke transform are AC values which, for control purposes, can lead to many problems since a reference for these values would need to be constantly changing. The Park transform solves this by converting the stationary reference frame with the alpha and beta currents to a rotating frame with DC the DC currents d and q. Besides the values of the alpha and beta currents, this conversion also needs the ω angle correspondent to the position of the rotating field on the air gap of the motor.

The Park transform is mathematically implemented by the matrix that follows [6].

$$i_{dq0}(t) = \begin{bmatrix} \cos(\theta) & \sin(\theta) & 0 \\ -\sin(\theta) & \cos(\theta) & 0 \\ 0 & 0 & 1 \end{bmatrix} \cdot \begin{bmatrix} i_{\alpha}(t) \\ i_{\beta}(t) \\ i_0(t) \end{bmatrix} \quad (2.9)$$

From the i_d and i_q currents it is possible to obtain a DC value for the whole current of the motor. From equation 2.5 and 2.6 it is possible to realize that the alpha and beta RMS values are the same as the RMS value of the currents i_a , i_b and i_c and based on the matrix in 2.9 it is possible

to realize that the value of the d and q currents will also be I when both of them are equal. With this, the value of the motors current is:

$$I_s = \sqrt{i_d^2 + i_q^2} \Leftrightarrow I_s = \sqrt{I^2 + I^2} = \sqrt{2} \cdot I \quad (2.10)$$

Just like the Clarke transform, Park's transform can also be reversed in order to obtain the alpha and beta currents that are equivalent to a set of d and q currents. This inverse transform is done with the next expression:

$$i_{\alpha\beta 0}(t) = \begin{bmatrix} \sin(\theta) & \cos(\theta) & 1 \\ \sin(\theta - \frac{2\pi}{3}) & \cos(\theta - \frac{2\pi}{3}) & 1 \\ \sin(\theta + \frac{2\pi}{3}) & \cos(\theta + \frac{2\pi}{3}) & 1 \end{bmatrix} \cdot \begin{bmatrix} i_d(t) \\ i_q(t) \\ i_0(t) \end{bmatrix} \quad (2.11)$$

The Park and Clarke transforms can be combined into a single matrix that enables the direct transformation between the three phase stationary reference frame and the dq rotating reference. This direct transformation is done with [7]:

$$i_{dq0}(t) = \frac{2}{3} \cdot \begin{bmatrix} \cos(\theta) & \cos(\theta - \frac{2\pi}{3}) & \cos(\theta + \frac{2\pi}{3}) \\ -\sin(\theta) & -\sin(\theta - \frac{2\pi}{3}) & -\sin(\theta + \frac{2\pi}{3}) \\ \frac{\sqrt{2}}{2} & \frac{\sqrt{2}}{2} & \frac{\sqrt{2}}{2} \end{bmatrix} \cdot \begin{bmatrix} i_a(t) \\ i_b(t) \\ i_c(t) \end{bmatrix} \quad (2.12)$$

2.3 Induction Motor

Induction motors have been in use for over a century and thus a a very developed technology. Because of the time during which the motor has been extensively improved, it now has most of the market share of electric motors, especially in high power usages [8].

Some of the main advantages of this kind of motor are its very low production costs, when compared to permanent magnets, mostly due to the lack of permanent magnets, the fact that this type of motor is able to achieve larger power outputs than permanent magnet and reluctance motors which makes them ideal for applications such as the railway. Induction motors are also controllable across a large range of speeds thanks to their field weakening capabilities [9].

On the other hand, induction motors have lower efficiency than synchronous motors and present a lower power factor that leads to higher power consumption for the same work developed [9].

Induction motors have two operating regions, a constant torque region and a constant power region. The constant torque region goes from 0rpm up until the motor reaches its synchronism frequency where the nominal flux of the motor is obtained by applying the motor's nominal voltage to its terminals. When the motor is at the synchronism speed the voltage can not be increased any further and given that it is intended to increase the frequency of the rotor the flux generated will decrease, since it is dependent on the $\frac{V}{F}$ ratio. The decrease of the flux will consequently lead to a decrease in torque [10].

The controllers that are developed for induction motors rely on the estimation of the torque and flux of the motor. The torque in the air gap of an induction motor can be written as:

$$T_{air-gap} = \frac{3}{2} \cdot p \cdot \Psi_s \times i_s \quad (2.13)$$

The flux of the motor can be expressed as:

$$\Psi_s = \int_0^t (u_s - R_s \cdot i_s) \cdot dt \quad (2.14)$$

This technique requires the calculation of the i_d and i_q currents which needs the calculation of the angle of the flux in the air gap. Because of this, the flux and torque can be calculated using equivalent expressions that use the alpha and beta currents. Using those currents the torque and flux are expressed as follows.

$$T_{air-gap} = \frac{3}{2} \cdot p \cdot \left(\Psi_{s\alpha}(t) \cdot i_{s\beta}(t) - \Psi_{s\beta}(t) \cdot i_{s\alpha}(t) \right) \quad (2.15)$$

$$\Psi_{s\alpha} = \Psi_{s\alpha}(0) + \int_0^t (u_{s\alpha} - R_s \cdot i_{s\alpha}) \cdot dt \quad (2.16)$$

$$\Psi_{s\beta} = \Psi_{s\beta}(0) + \int_0^t (u_{s\beta} - R_s \cdot i_{s\beta}) \cdot dt \quad (2.17)$$

From equations 2.16 and 2.17, it is possible to calculate the value of the flux as well as the angle of the flux in the air gap of the motor. These two values are calculated as follows in the next expressions, respectively:

$$\Psi_s = \sqrt{\Psi_{s\alpha}^2 + \Psi_{s\beta}^2} \quad (2.18)$$

$$\theta = \arctan \left(\frac{\Psi_{s\alpha}}{\Psi_{s\beta}} \right) \quad (2.19)$$

2.4 Energy Storage System

To implement an on-board energy storage system there are two main components required, the storage devices and a converter that charges or discharges the storage device depending on the train's power requirements. To achieve this, many technologies of storage devices are available and the most relevant will be discussed in this section.

This system needs to be able to store enough energy to cut all the power peaks from the catenary and also needs to be able to discharge at a rate high enough to supply the necessary power. Beyond this, the storage device must be small enough to be fitted on a train and the number of charge/discharge cycles it supports must be high enough to guarantee its durability.

The most common storage devices are batteries due to their capability to store large amount of energy per volume when compared to other solutions. Table 2.1 presents a preliminary analyses to different types of batteries [4].

	Energy Density (Wh/kg)	Cycle life (number of cycles)	Operating Range Temperature ($^{\circ}C$)
Lead	30-50	400-1200	-20° to 60°
Ni-Cd	45-80	2000	-40° to 60°
Ni-Mh	60-120	1500	-20° to 60°
Ni-Zn	60-85	1000	-20° to 60°
Zebra	100-140	>1000	270° to 350°
Redox	10-20	>10000	10° to 40°
Li-Ion	110-160	1000	-20° to 60°
Li-Polymer	110-160	1000	-20° to 60°

Table 2.1: Energy density, cycle life and operating temperature of batteries [4]

Given the requirements previously mentioned for the storage device, the batteries that use the technologies lead, Ni-Cd, Ni-Zn and Redox are not suitable for this project due to their low energy density. The implementation of this battery technologies would make the system too bulky and heavy to be a feasible solution.

The battery based on the Zebra technology, even though it presents good values for the energy density and number of life cycles, is not practical for the application intended due to the operating temperature requirements. This battery type is part of the molten-salt battery technologies which uses liquid salts in its composition. This implies that the temperature of operation need to be high enough to melt the salt which makes it unusable in this context [11].

Lithium Polymer batteries, despite having attractive characteristics are not usable for large batteries because their cost would make the project unviable.

For the project at study, the two technologies that may be suitable for an implementation are the Nickel-metal hydride and the Lithium-Ion technologies. These two technologies will be further analysed in order to find the most suitable for this implementation.

Nickel-metal hydride batteries have seen over the last few years a great increase in their power from 200 to 1200 W/kg. The operating temperature range has also increased allowing this type of battery to maintain optimal power through all their operating range with some newer advancements even expanding that range to $-30^{\circ}C$ to $70^{\circ}C$. Other advantages of this technology are the flexibility in the cells size, safe operation at voltages above 320V, the flexibility in the module's configuration, the capability to operate under abusive charge and discharge rates, which facilitates applications like regenerative braking. Furthermore this technology enables the use of simple charging solutions and the materials used in their construction are not as toxic as the ones used in other technologies. Despite all these qualities, most of these advancements are still very recent and the products available in the market have some deficiencies that must be overcome [12].

In [13] a solution to supply power during the acceleration process is presented. This battery pack has a capacity of 1 to 2 kWh and can be charged in a small amount of time and then provide

power to the traction system when the speed needs to be increased. The Osaka Municipal Transportation Bureau has also implemented a large scale battery of this type capable of delivering a power of 5.6MW and store 576kWh

Lithium-Ion batteries provide the highest energy density of all the technologies [14]. This makes this technology ideal for applications where weight and volume are critical conditions. Lithium-Ion batteries, when compared to Ni-Mh, have a voltage per cell about three times higher, which reduces significantly the number of cells required to achieve high voltage modules [14]. A major problem with Li-Ion batteries is the high toxicity of its materials, in case of an accident these batteries combustion generates more than 100 toxic gases. These accidents can be prevented but, if safety measures are not considered, the overcharging of the cells can lead to temperature rises that may ignite the flammable materials that make the cells [15]. Because of these Li-Ion cells require special packing to contain and prevent incidents. One of the required systems to prevent accidents is a battery management system that balances the charge of all cells preventing overcharges [16].

Some solutions with this technology have been implemented around the world in the railways. The approaches used range from small batteries with a storage capability of just 18.1kWh and 250kW of power to large batteries with 140kWh of capacity and a power of 1.05MW [13].

Batteries are not the only storage device that can be used in this application, supercapacitors can also be a relevant technology to consider, mainly due to the high power requirements of a large vehicle like a train. Supercapacitors have a charge time more than sixty times lower than a Li-Ion battery which enables very high powers, ideal for regenerative braking and fast accelerations. Supercapacitors also have a number of lyfe cycles that be up to 1000 times greater than the one of Li-Ion increasing the durability of the energy storage system significantly. These qualities come with some disadvantages such as its price per kWh that is currently between five and ten times higher than the equivalent capacity of Li-Ion batteries. The energy density of these capacitors is also significantly lower than its lithium ion counterparts, making their implementation heavier and bulkier [17].

Due to the many favourable points for both the supercapacitors and the lithium ion batteries, both of the solutions will be further studied during this dissertation.

2.5 Regenerative Breaking

Regenerative breaking is one of the technologies with the greatest energy savings potential and combined with an energy storage system it can achieve energy savings of up to 30% for rail transports [1].

In order to store the energy generated during braking periods, used to reduce speed or to maintain it while going in rail stretches with negative slope, it is necessary to implement a converter that transfers the energy from the DC link to the ESS (battery or supercapacitor).

The voltage of the ESS can have a higher or a lower value than the voltage on the DC link and based on the approach used, the configuration of the converter must differ to obtain the intended

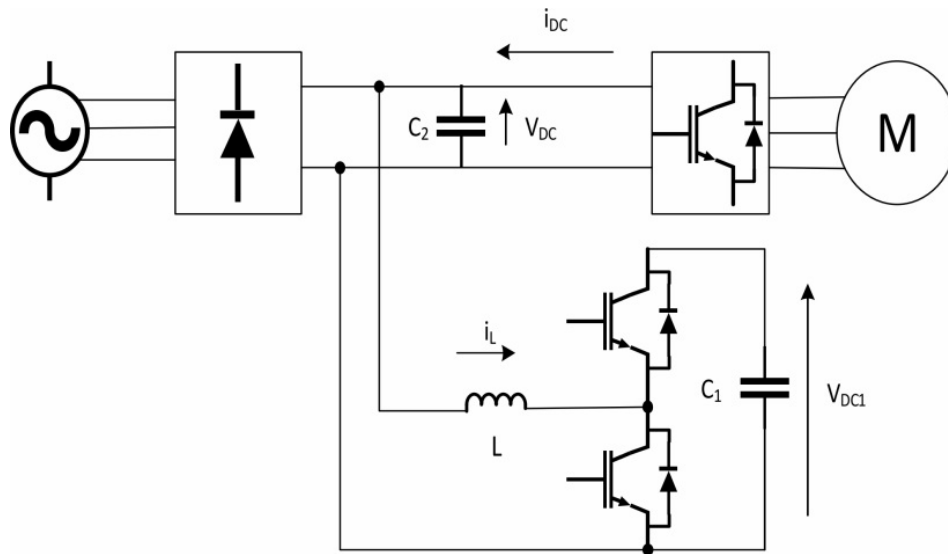


Figure 2.1: High voltage ESS bidirectional Charging/Discharging converter[1]

behaviour from the circuit. The converter used to charge the ESS is the same that is used when the ESS supplies power to the DC link in order to reduce the power necessary from the catenary [1].

2.5.1 High Voltage ESS

In a configuration where the ESS is at a higher voltage than the DC link, the converter must be a bidirectional DC/DC converter that behaves as a step-up converter from the DC-link to the ESS and a step-down converter in the opposite direction. The solution presented in [1] is shown in figure 2.1.

When charging the ESS the converter behaves like a boost converter and the current i_L is positive, increasing the charge in the ESS. When the motors require more power for acceleration the converter behaves as a buck and the current on the inductor becomes negative discharging the ESS and providing charge to the DC-link. For the charge process the converter uses the bottom transistor and the top diode and to discharge the ESS the top transistor is commanded and the current flows through it and the bottom diode.

2.5.2 Low Voltage ESS

For this configuration the circuit operates in the opposite manner as the one on the high voltage ESS. When the vehicle is generating power due to electric braking, the converter acts as a step-down leading charge from the DC-link to the ESS. When the traction system requires more power the converter acts as a step-up converter transferring charge from the ESS to the DC-link [1, 18]. This circuit is illustrated in figure 2.2.

During the ESS charging process the converter acts as a buck converter with the top transistor and bottom diode, leading to a positive i_L current, discharging the DC-link and charging the ESS.

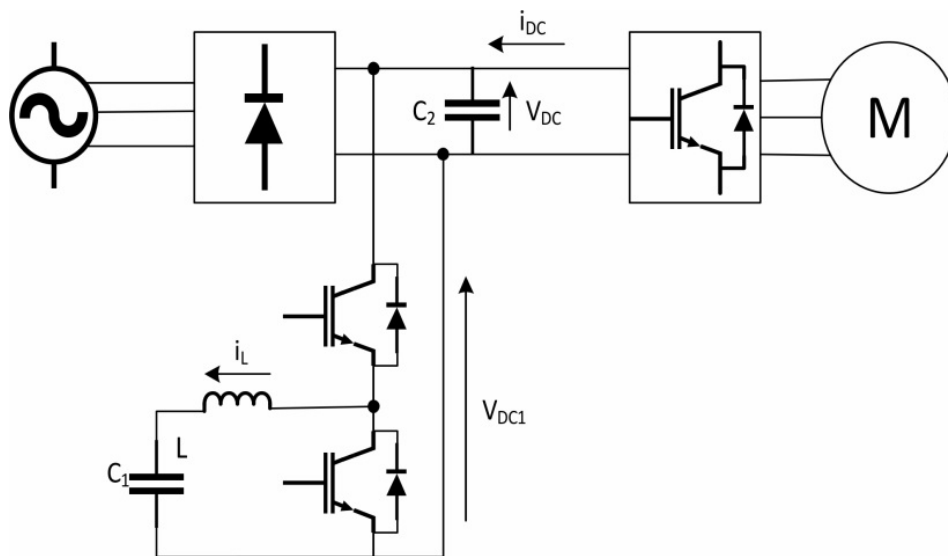


Figure 2.2: Low voltage ESS bidirectional Charging/Discharging converter [1]

When the motor requires peaks of power, the converter acts as a boost converter and, with the bottom transistor and top diode, the battery charges the DC link, turning the i_L current negative.

2.5.3 Charging Control

Since the traction inverter already existing in the series 4000 train (known as alfa pendular) uses transistors, there is no need to adjust the control of the power train itself to implement this feature.

It is required a controller for the battery charging/discharging system. This controlled is based on a current controller that has the goal to maintain the voltage of the DC link at the desired value [18].

Considering that typical OESS have voltages under 1000V, mostly for safety reasons, and that the voltage of the trains DC link is 2200V, the topology that is adequate for the implementation at study in this dissertation will be the low voltage ESS.

2.6 Photovoltaic Panels

Photovoltaic panels work on the principle that, when sun light is focused on the solar cells, the electrons in the atoms that make the cell absorb the energy from the sun light and are released from the atomic nucleus electric field. This process generates multiple free electrons in the solar cells thus generating electricity [19].

There are many different technologies currently used for the solar cells with the most common being monocrystalline silicon, polycrystalline silicon, amorphous silicon, copper indium diselenide and cadmium telluride [19, 20].

Monocrystalline solar panels, as the name implies, are made of solar cells that are each a single silicon crystal [21]. The production mechanisms required to manufacture the large crystals

required by these cells is complex and leads to low yields of the material, making this technology the most expensive [20, 22]. This technology presents the highest efficiency of all the existing technologies (around 19%) [22].

Polycrystalline solar panels are made by melting silicon crystals together to make the wafers. This production technique is simpler than the one required to make monocrystalline cells and thus, guarantees higher yields on the manufacturing process and a lower overall cost [20]. Although this technology is significantly cheaper than the monocrystalline one, the efficiency of the cells is also significantly lower (peaking at 14%) [22].

Based on the work developed in [20] it's possible to evaluate other characteristics of the mono and polycrystalline panels, beyond just their efficiency. Monocrystalline panels are over 50% more efficient than polycrystalline under temperature variations of 60°C which allows monocrystalline panels to operate more efficiently in conditions of high temperature, that tend to have higher temperatures. Monocrystalline cells also have the advantage of performing better under low solar radiation conditions [20].

The flexible cell technologies, despite having a lower efficiency than their more mature technologies counterparts, have had a large qualitative leap in the last few years and their efficiency is already above 15%. Other than that, their shape and flexibility can have great advantages for some specific applications due to their ability to adjust to the surface where they are mounted and the fact that they have a very reduced profile.

Considering this dissertation purpose, and the fact that aerodynamic forces have a very big impact on high speed movement, the flexible cell solar panels are the most adequate for this implementation. Even though the energy generated is not as high as with other technologies, if other non flexible panels were used, the increase in power usage due to aerodynamic forces would surpass largely their benefits.

Chapter 3

Simulation Model

3.1 Summary

For a correct and accurate simulation, the train model and all its components must be well defined. This chapter will start by presenting a complete physical model of the train characterising all its parameters that are considered essential. Then the power converter from both the traction and the auxiliary system will be presented along with their respective controllers that guarantee the train's correct operation.

3.2 Physical Model

A train is subject to multiple forces that have a direct impact on the way the train's speed varies during a given stretch of track. These forces can be separated into two groups, the forces that contribute to the motion of the vehicle (Traction Forces) and those that are opposed to its motion. To establish a physical model of the train movement implies to characterize both the forces.

3.2.1 Resistive Forces

The minimum force that must be applied to the train in order for it not to decelerate, and thus maintain its speed constant, corresponds to the sum of all the forces that oppose the movement of the vehicle for a given velocity. Those can be represented by the sum of the friction forces between the wheels and the track, the friction forces between all the mechanical components that link the motors to the wheels and the force inherent to the aerodynamic drag [23].

$$F_R = F_M + F_D \quad (3.1)$$

In order to describe all the resistive forces acting on a vehicle when it is traveling at a specific speed, the equation, consistently used throughout the literature for almost a century is the one firstly presented by Davis in 1926 [24].

$$F_R = A + Bv + Cv^2 \quad (3.2)$$

For this equation the parameter A represents the resistance component that is constant with the changes in speed, the parameter B incorporates the resistances that are proportional with the speed. The parameter C corresponds to the resistances that vary with the square of the velocity that are a consequence of the aerodynamic drag [24].

To obtain the values of the three constants requires that some physical tests are performed and data is collected and analysed. Based on the work developed by Lukaszewicz in 2001 [23], which consisted on performing a series of tests with multiple trains, in order to obtain values for the constants A, B and C. The series 4000 train, at study in this dissertation, has characteristics that are very similar to those of the X2 train present in Lukaszewicz's experimental work and thus can be considered for this case study. From this, the A, B and C parameters of the series 4000 train are as follows:

$$A = 2000 \quad (3.3)$$

$$B = 40 \quad (3.4)$$

$$C = 6.9 \quad (3.5)$$

The model presented up to this point does not take into consideration the existence of grades on the track. In order to incorporate those into the simulation model the resistance imposed by the force of gravity, during an inclined stretch, must be considered [25]. This force can be described by the following equation:

$$F_G = Mgsin(\theta) \quad (3.6)$$

Having this force, the total resistive force applied to the train can be calculated as:

$$F = F_R + F_G \quad (3.7)$$

By combining the equation 3.7 with the equations 3.2 and 3.6 it is possible to describe the resistive forces applied to the train as a function of its velocity and the angle of the terrain in which the tracks are laid.

$$F = A + Bv + Cv^2 + Mgsin(\theta) \quad (3.8)$$

As the mass of the complete train with six carriages and filled with passengers is 298.3 tons [26], equation 3.8 becomes:

$$F = 2000 + 40 \cdot v + 6.9 \cdot v^2 + 298300 \cdot 9.8 \cdot \sin(\theta) \quad (3.9)$$

From this equation it is possible to visualize the drag forces impacting on the vehicle for any given moving velocity.

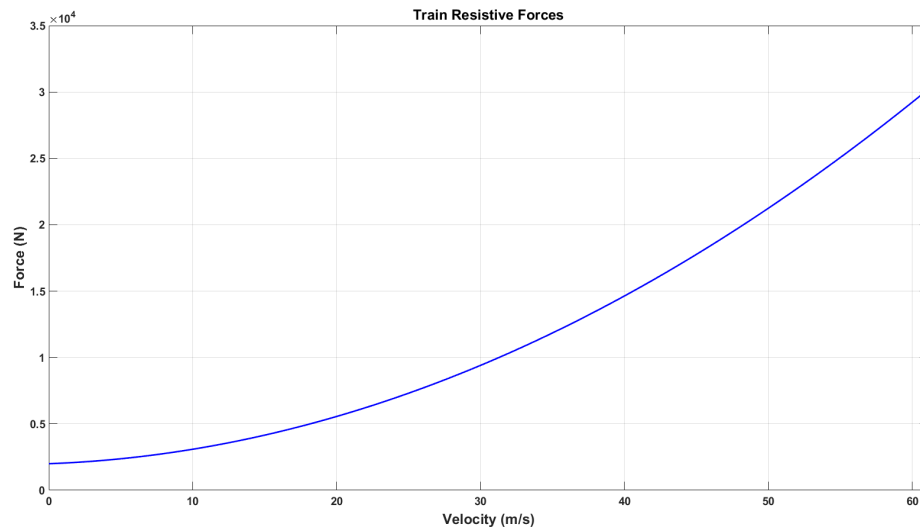


Figure 3.1: Resistive Forces across the operating speed range

The mechanical power required to maintain the train's speed can be expressed by the following equation: [27]:

$$P_{mec} = F \cdot v \quad (3.10)$$

Combining equation 3.10 with equation 3.9 the power required by the train to maintain a constant travel speed is:

$$P_{mec} = 2000 \cdot v + 40 \cdot v^2 + 6.9 \cdot v^3 + 298300 \cdot 9.8 \cdot \sin(\theta) \cdot v \quad (3.11)$$

From this equation it is possible to obtain the torque value that corresponds to a 0 m/s² acceleration for any given velocity and terrain grade, by means of the following expression:

$$T = \frac{P_{mec}}{\omega} \quad (3.12)$$

$$T = \frac{2000 \cdot v + 40 \cdot v^2 + 6.9 \cdot v^3 + 298300 \cdot 9.8 \cdot \sin(\theta) \cdot v}{\omega} \quad (3.13)$$

Knowing the radius of the wheels of the train, the ω value can be converted into a proportion of the train's velocity:

$$\omega = \frac{2\pi \cdot v}{2\pi \cdot r} = \frac{v}{r} \quad (3.14)$$

Merging equation 3.13 with equation 3.14 the torque is given as:

$$T = \frac{2000 \cdot v + 40 \cdot v^2 + 6.9 \cdot v^3 + 298300 \cdot 9.8 \cdot \sin(\theta) \cdot v}{v} \cdot r \quad (3.15)$$

$$\Leftrightarrow (2000 + 40 \cdot v + 6.9 \cdot v^2 + 298300 \cdot 9.8 \cdot \sin(\theta)) \cdot r \quad (3.16)$$

Just by observation it is possible to conclude that the torque can also be written as:

$$T = F \cdot r \quad (3.17)$$

Replacing the radius by its value:

$$T = (2000 + 40 \cdot v + 6.9 \cdot v^2 + 298300 \cdot 9.8 \cdot \sin(\theta)) \cdot 0.445 \quad (3.18)$$

Applying equations 3.9, 3.11 and 3.18 with the train's nominal velocity (220km/h or 61.11m/s) it is possible to obtain the values of Force, Power and Torque required to maintain the train in a steady state at peak velocity. Those values are as follows:

$$F = 2000 + 40 \cdot 61.11 + 6.9 \cdot 61.11^2 + 298300 \cdot 9.8 \cdot \sin(0^\circ) = 30.2kN \quad (3.19)$$

$$P = 2000 \cdot v + 40 \cdot 61.11^2 + 6.9 \cdot 61.11^3 + 298300 \cdot 9.8 \cdot \sin(0^\circ) \cdot 61.11 = 1.85MW \quad (3.20)$$

$$T = (2000 + 40 \cdot 61.11 + 6.9 \cdot 61.11^2 + 298300 \cdot 9.8 \cdot \sin(0^\circ)) \cdot 0.445 = 13.4kN \cdot m \quad (3.21)$$

The maximum resistive forces acting on the train, at a constant velocity, will occur when it is rolling up an incline with the maximum admissible value, 1%. For these conditions the values of Force, Power and Torque required to maintain the velocity unchanged will be:

$$\alpha = \arctan(0.01) = 0.573^\circ \quad (3.22)$$

$$F = 2000 + 40 \cdot 61.11 + 6.9 \cdot 61.11^2 + 298300 \cdot 9.8 \cdot \sin(0.573^\circ) = 59.4kN \quad (3.23)$$

$$P = 2000 \cdot v + 40 \cdot 61.11^2 + 6.9 \cdot 61.11^3 + 298300 \cdot 9.8 \cdot \sin(0.573^\circ) \cdot 61.11 = 3.63MW \quad (3.24)$$

$$F = (2000 + 40 \cdot 61.11 + 6.9 \cdot 61.11^2 + 298300 \cdot 9.8 \cdot \sin(0.573^\circ)) \cdot 0.445 = 26.5kN \cdot m \quad (3.25)$$

From these values, it is possible to conclude that just a small grade on the tracks like 1%, requires almost twice the power than the same speed profile on a flat terrain. On such an incline the train will be at 90.82% of its nominal power of 4MW.

3.2.2 Traction Force

A series 4000 train is able to produce 210kN of force, at the wheels, when the induction motors are working in the constant torque region of operation. At its maximum velocity (220km/h) the force transformed into movement can be defined as:

$$F_{V_{max}} = \frac{P_{max}}{V_{max}} \quad (3.26)$$

By applying the equation to the known values, the maximum force applied to the train at its maximum speed is:

$$F_{V_{max}} = \frac{4000000}{61.11} = 65.5kN \quad (3.27)$$

From the two force values presented, it is possible to determine the speed of the train at which the motors achieve their nominal speed and begin operating in a field weakening region. This velocity can be determined by applying the equation:

$$V_{synchronism} = \frac{F_{V_{max}} \cdot V_{max}}{F_{max}} \quad (3.28)$$

By applying the previously stated values to the formula:

$$V_{synchronism} = \frac{65455.74 \cdot 61.11}{210k} = 19.0476m/s = 68.6km/h \quad (3.29)$$

With this value a traction force graphic can be designed in order to display the force available for any given speed in the desired speed range.

The traction force curve is described by the equation system that follows:

$$F_T = \begin{cases} 210000N, & v \leq V_{synchronism} \\ \frac{V_{max} \cdot F_{V_{max}}}{v}, & v > V_{synchronism} \end{cases} \quad (3.30)$$

According to [28], the maximum force delivered to the train at its maximum velocity is 69.5kN, which is slightly above the calculated value. Using this force value, it is possible to analyse the values of Power and Torque at the maximum speed, by applying equations 3.10 and 3.17, respectively.

$$P = 69.5k \cdot 61.11 = 4.25MW \quad (3.31)$$

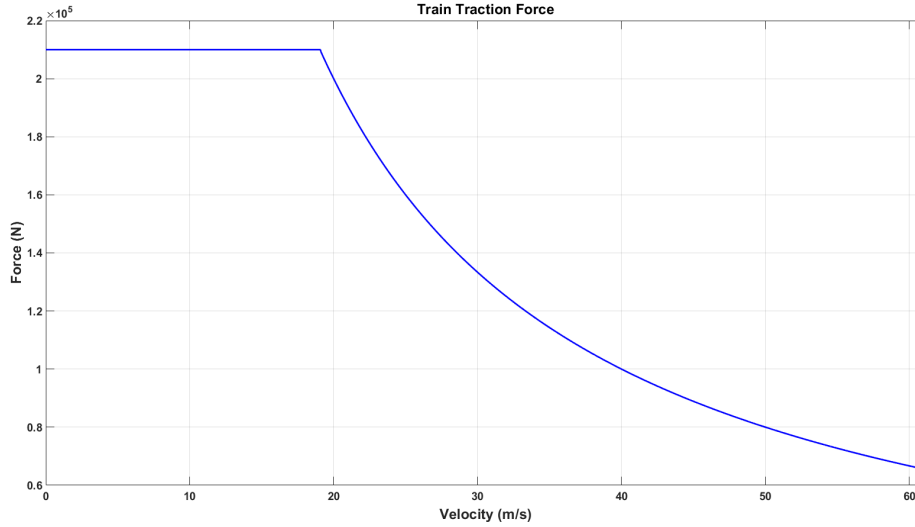


Figure 3.2: Traction Force across the operating speed range

$$T = 69.5k \cdot 0.445 = 30.9kN \cdot m \quad (3.32)$$

At the maximum velocity the mechanical power delivered to the wheels surpasses the nominal power produced by the motors. This can be explained by the control method used for these motors, in the field weakening region of the motors the direct current (responsible for the production of flux) is reduced in order to maintain the reason V/F of the motor constant and thus the quadrature current (responsible for the production of torque) can be slightly increased while still maintaining the motor at a nominal current level.

For last, the traction and velocity values can be used to calculate the gearbox ratio required to operate the train within the intended parameters. Assuming a nominal frequency of the current on the stator of 50Hz, a slip frequency of 1.3% and two pole pairs, when the train is travelling at 19.0476m/s the frequency of the rotor must be given by the formula:

$$F_{rotor} = \frac{f_n}{p} \cdot (1 - s) \quad (3.33)$$

Replacing the variables with their values, the frequency of the rotor when the train travels at 19.0476m/s is:

$$F_{rotor} = \frac{50}{2} \cdot (1 - 0.013) = 24.675Hz = 49.35\pi rad/s \quad (3.34)$$

The frequency of the wheels, when the train is travelling at 19.0476m/s is given by the following expression:

$$F_{wheels-50Hz} = \frac{V_{synchronism}}{2 \cdot \pi \cdot r} \quad (3.35)$$

By replacing the variables with their values, the Frequency of the wheels is:

$$F_{wheels-50Hz} = \frac{19.0476}{2 \cdot \pi \cdot 0.445} = 6.81Hz = 42.80rad/s \quad (3.36)$$

Having all these parameters, the ideal gearbox ratio that will meet the imposed criteria can be calculated by means of the next equation:

$$GB_{ratio} = \frac{F_{rotor}}{F_{wheels-50Hz}} \quad (3.37)$$

Replacing the calculated frequencies in the equation, the gearbox ratio must be:

$$GB_{ratio} = \frac{24.675}{6.81} = 3.62 \quad (3.38)$$

Considering the torque values across the speed range of the train and the gearbox ratio, it is possible to determine the torque produced by each motor.

$$T_m = \frac{T}{N_{mot} \cdot GB} \quad (3.39)$$

With this expression, and expression 3.16 the values for the maximum torque (on the constant torque region of the motors), and the torque at the maximum velocity can be calculated.

$$T_{m-0} = \frac{210k \cdot 0.445}{8 \cdot 3.62} = 3226.86N \cdot m \quad (3.40)$$

$$T_{m-v_{max}} = \frac{65455.74 \cdot 0.445}{8 \cdot 3.62} = 1005.79N \cdot m \quad (3.41)$$

3.2.3 Train Movement

3.2.3.1 Acceleration

Up to this point only constant speed operation was analysed but the most critical operation points of the train are the ones when there is an acceleration different from $0m/s^2$. During the acceleration and deceleration processes the traction force required to be produced by the power train is different than the one from the resistive forces. The difference between those two forces corresponds to the acceleration force and, by applying Newton's second law of motion, the acceleration of the train can be obtained [25].

$$F_{accel} = F_T - F \quad (3.42)$$

$$accel = \frac{F_{accel}}{m} \quad (3.43)$$

Even though the applied force to the train, to induce a velocity change, can vary, the most efficient way to accelerate and decelerate a vehicle is by doing it in the least time possible. With this approach the train achieves the top speed required to meet a deadline faster, which leads to a lower maximum velocity required to meet that deadline. Since the drag forces applied to the train

increase as the square of the velocity, the lower the top speed required to meet a deadline, the more efficient the journey will be.

Having made this consideration, the force applied to the train during an acceleration process will correspond to the maximum traction force the train is able to produce at a given velocity, as can be seen in figure 3.2 and equation 3.30.

By combining the equation 3.42 with equations 3.30 and 3.9, the expression that characterizes the force responsible for the acceleration of the train can be obtained as a function of the train's instantaneous velocity.

$$F_{accel} = \begin{cases} F_{Tmax} - (a + b \cdot v + c \cdot v^2 + m \cdot g \cdot \sin(\theta)), & v \leq V_{synchronism} \\ \frac{V_{max} \cdot F_{Vmax}}{v} - (a + b \cdot v + c \cdot v^2 + m \cdot g \cdot \sin(\theta)), & v > V_{synchronism} \end{cases} \quad (3.44)$$

Replacing the constants by their values the following is obtained:

$$F_{accel} = \begin{cases} 210000 - (2000 + 40 \cdot v + 6.9 \cdot v^2 + 298300 \cdot 9.8 \cdot \sin(\theta)), & v \leq 19.0476m/s \\ \frac{4000000}{v} - (2000 + 40 \cdot v + 6.9 \cdot v^2 + 298300 \cdot 9.8 \cdot \sin(\theta)), & v > 19.0476m/s \end{cases} \quad (3.45)$$

Joining equation 3.43 with equation 3.45 the maximum acceleration of the train, while traveling at a specific velocity, can be obtained, as follows in the expression:

$$accel_{max}(v) = \begin{cases} \frac{210000 - (2000 + 40 \cdot v + 6.9 \cdot v^2 + 298300 \cdot 9.8 \cdot \sin(\theta))}{298300}, & v \leq 19.0476m/s \\ \frac{4000000}{298300 \cdot v} - \frac{(2000 + 40 \cdot v + 6.9 \cdot v^2 + 298300 \cdot 9.8 \cdot \sin(\theta))}{298300}, & v > 19.0476m/s \end{cases} \quad (3.46)$$

From this equation, the maximum acceleration felt by the train can be calculated, and this value will occur when the velocity is 0m/s since at this moment the traction force that can be exerted is maximum and the resistive forces acting on the train are minimum. For this calculation the gradient of the terrain is considered as 0°.

$$accel_0 = \frac{210000 - 2000}{298300} = 0.6973m/s^2 \quad (3.47)$$

Based on equation 3.46 an equation can be written in order to describe the velocity variation of the train through time during an acceleration. This equation is described as follows.

$$v_t = v_{t-1} + \dot{v}_{t-1} \cdot dt = v_{t-1} + accel_{max}(v_{t-1}) \cdot dt \quad (3.48)$$

Since the acceleration of the train, for any given speed inside the nominal operating range of the velocity, is known through equation 3.46, equation 3.48 can be written as:

$$v_t = \begin{cases} v_{t-1} + \frac{210000 - (2000 + 40 \cdot v_{t-1} + 6.9 \cdot v_{t-1}^2 + 298300 \cdot 9.8 \cdot \sin(\theta))}{298300} \cdot dt, & v_{t-1} \leq 19.0476m/s \\ v_{t-1} + \left(\frac{4000000}{298300 \cdot v_{t-1}} - \frac{2000 + 40 \cdot v_{t-1} + 6.9 \cdot v_{t-1}^2 + 298300 \cdot 9.8 \cdot \sin(\theta)}{298300} \right) \cdot dt, & v_{t-1} > 19.0476m/s \end{cases} \quad (3.49)$$

This equation can be implemented in a simple program A.1, C coded one, in order to calculate the time the train requires to achieve a given speed while starting at a lower one. Considering that the velocity of the train has a slow variation, the time delta used between iterations can be considered as 1 second. Reducing this time will lead to an increased precision of the calculations. From the execution of this code with different time deltas, the following values were obtained for acceleration from a standstill to the maximum velocity of 61.1111m/s.

Time Step(s)	Final Time(s)	Final Velocity(m/s)	Velocity Error(m/s)
10	200	62.1698	1.0587
1	199	61.1346	0.0235
0.1	199.7	61.1203	0,0092
0.01	199.70	61.1112	0.0001
0.001	199.719	61.1112	0.0001

Table 3.1: Calculated acceleration times from standstill to top speed with multiple step sizes

As the results show, even with a large step size, the values obtained are very precise presenting an error under 2%. The results also indicate that a complete acceleration of a series 4000 train takes 183.32 seconds to achieve its maximum velocity while travelling on a flat terrain.

3.2.3.2 Braking

When the train needs to reduce its speed and brake, instead of using mechanical brakes, it can take advantage of the electric braking capability of the motors, in order to store energy and to reduce the wear of the mechanical brakes. From [28] it is known that the force available for braking purposes is 79% of the one that can be used for acceleration purposes. During braking, the resistive forces will work in favour of the braking system helping the train to stop faster – in fact it is possible to recover the kinetic energy, in a mechanical form, as electric energy usable in future acceleration/traction condition. From this, an equation describing the forces applied on the train can be written as:

$$F_{decel} = F_{brake} + F = 0.79 \cdot F_T + F \quad (3.50)$$

Joining equations 3.9 and 3.30 to equation 3.50, an equation describing the braking force exerted on the train in relation to the instantaneous velocity can be obtained.

$$F_{decel} = \begin{cases} 0.79 \cdot F_{Tmax} + a + b \cdot v + c \cdot v^2 + m \cdot g \cdot \sin(\theta), & v \leq V_{synchronism} \\ \frac{0.79 \cdot V_{max} \cdot F_{Vmax}}{v} + a + b \cdot v + c \cdot v^2 + m \cdot g \cdot \sin(\theta), & v > V_{synchronism} \end{cases} \quad (3.51)$$

The deceleration to which the train is subjected at a given speed, when braking is given by:

$$decel = \frac{F_{decel}}{m} \quad (3.52)$$

By combining equation 3.51 with equation 3.52 the instantaneous velocity variation, when traveling at a specific speed, is:

$$decel_{max}(v) = \begin{cases} 0.79 \cdot F_{Tmax} + a + b \cdot v + c \cdot v^2 + m \cdot g \cdot \sin(\theta), & v \leq V_{synchronism} \\ \frac{0.79 \cdot V_{max} \cdot F_{Vmax}}{v} + a + b \cdot v + c \cdot v^2 + m \cdot g \cdot \sin(\theta), & v > V_{synchronism} \end{cases} \quad (3.53)$$

The constants in this equation can be replaced by their values, and thus, making the equation only dependent on the velocity and the inclination of the terrain, it becomes:

$$decel_{mx}(v) = \begin{cases} 53710.03 + 40 \cdot v + 6.9 \cdot v^2 + 298,3k \cdot 9.8 \cdot \sin(\theta), & v \leq 19.0476m/s \\ \frac{0.79 \cdot 4000k}{v} + 2k + 40 \cdot v + 6.9 \cdot v^2 + 298,3k \cdot 9.8 \cdot \sin(\theta), & v > 19.0476m/s \end{cases} \quad (3.54)$$

Just like it was done in 3.48 it is possible to implement a similar expression that describes the velocity variation during the deceleration process.

$$v_t = v_{t-1} + \dot{v}_{t-1} \cdot dt = v_{t-1} - decel_{mx}(v_{t-1}) \cdot dt \quad (3.55)$$

Replacing the deceleration variable with the known expression presented in 3.55, the equations obtained to describe the behaviour of the train's velocity when braking are:

$$v_t = \begin{cases} v_{t-1} - \frac{0.79 \cdot 210000 + 2000 + 40 \cdot v_{t-1} + 6.9 \cdot v_{t-1}^2 + 298300 \cdot 9.8 \cdot \sin(\theta)}{298300} \cdot dt, & v_{t-1} \leq 19.0476m/s \\ v_{t-1} - \left(\frac{0.79 \cdot 4000000}{298300 \cdot v_{t-1}} + \frac{2000 + 40 \cdot v_{t-1} + 6.9 \cdot v_{t-1}^2 + 298300 \cdot 9.8 \cdot \sin(\theta)}{298300} \right) \cdot dt, & v_{t-1} > 19.0476m/s \end{cases} \quad (3.56)$$

By implementing the previous equations in a C program A.2 the deceleration time can be simulated and analysed, with the time step used defining the degree of precision of the values obtained. The following results represent a series 4000 train braking from 220km/h to a standstill.

Time Step(s)	Final Time(s)	Final Velocity(m/s)	Velocity Error(m/s)
10	170	-3.4315	3.4315
1	161	-0.0505	0.0505
0.1	160.6	-0.0072	0.0072
0.01	160.56	-0.0033	0.0033
0.001	160.571	0.0000	0.0000

Table 3.2: Calculated deceleration times from top speed to a standstill with multiple step sizes

Just like with the previous results, it is possible to see that the error is significantly reduced when the time step is reduced. These results, when compared to those of table 3.1, demonstrates the impact that resistive forces have on the performance of rail vehicles. Even though the braking capacity of the train is only 79% of its traction capacity, the time it takes for the train to completely brake from its maximum velocity is about 30% faster than the time required to achieve that maximum speed when starting at a standstill.

3.2.4 Matlab Implementation

In order to simulate the series 4000 train in Matlab/Simulink, it is necessary to transpose the physical model, presented up to this point, to the simulation platform. Taking advantage of the Vehicle Dynamics Blockset present in the software package, the block Vehicle Body Total Road Load was used, since it implements the exact same model that was analysed.

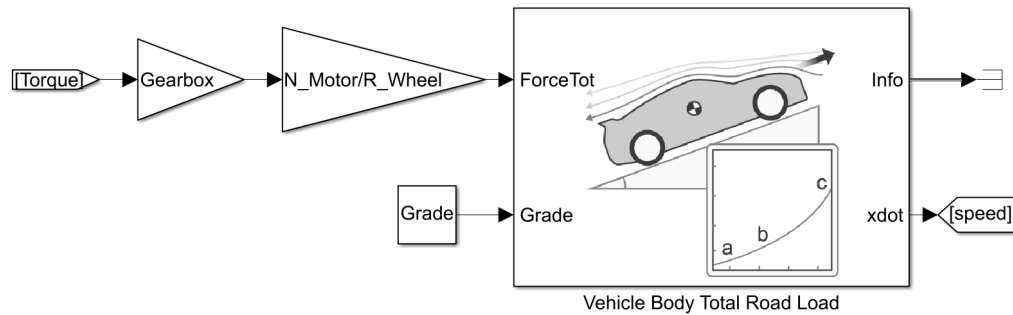


Figure 3.3: Matlab/Simulink implementation of the train's physical model

The inputs of this block are the terrain's grade and the traction or braking force that is being applied to the vehicle, produced by the motors. Since the output of the motor is a torque value, it is converted to force by means of equation 3.39. This value is also multiplied by the number of motors because it is assumed that all motors operate equally at all time. This is only done to optimize the simulation time, given that in reality the further back a motor is, the more force it is required to produce due to anti-slip of the wheels as well as the mechanical tension over connections between carriages. Since the purpose of this dissertation is to study the energy consumption of the train, this small difference between the motors can be overlooked as a simplification.

3.3 Micro Grid

A series 4000 train's micro grid is divided into two systems, the traction and the auxiliary. The traction subsystem contains all the necessary components that enable the motors to work, the auxiliary is responsible to deliver power to all the devices that require electrical power, other than the motors. These devices can be the Air-Conditioning units, the lights inside the carriages, the power sockets... These two systems are fed by a transformer with two secondary windings, which has its primary winding connected to a 25kV line through the catenary. The two secondary windings present in the transformer have an output voltage of 1500V and 600V for the traction and auxiliary systems, respectively.

In order to reduce the conduction losses on wires and for safety reasons, in case of failure, the train is divided into two equal micro-grids that each power half the carriages of the train. If one of the two grids has a problem the train can continue to operate in a reduced power mode, where the traction is limited to half the motors.

For the purposes of this dissertation, the train will be considered an insulated system that only receives power from the grid but doesn't send any power back. With this approach the simulated train is considered as the only load on the grid and, since the substations that powers the catenary can not transport power bidirectionally, all the energy that the train may be able to regenerate will either be stored in an OESS or it will be lost. This will be done in order to assess the maximum optimization that can be achieved only by implementing the systems that will be proposed in this dissertation.

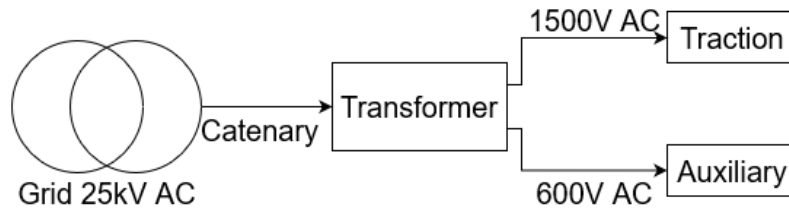


Figure 3.4: Train's micro grid general structure

3.4 Traction System

The traction subsystem of the electrical micro grid of a 4000 series train is composed of multiple electrical converters that have the goal to power the eight induction motors through all the operation modes required. This subsystem consists on linking a single phase AC/DC power converter in series with a three phase DC/AC power converter that delivers power to the motors. The AC/DC converter has an input of 1500V AC and generates a DC link of 2200V, which will then be used as the input for the three phase inverter that powers the motors.

3.4.1 AC/DC Converter

The AC to DC power converter consists of a single phase full bridge of transistors, with anti-parallel diodes, that switch at a set frequency. The converter also uses an input inductance and an output capacitor to filter the switching frequency. Since this converter is set at the end of the secondary winding of the AC/AC transformer, the leakage inductance of the transformer is used as part of the AC/DC converter.

The bridge used to implement this converter, with the adequate control, enables bidirectional power conversion but, given the study that is intended to be done throughout this dissertation, only the AC to DC direction will be considered.

For this application the voltage of the DC Link is intended to be higher than any value of the 1500V AC source (2121V peak), this circumstance leads to the need to operate the converter in a similar manner as a DC/DC boost converter.

When the sinusoidal source (in series with the inductor simulates the AC/AC transformer) has a positive value, the left arm of the bridge is used for the power conversion. The transistor T2

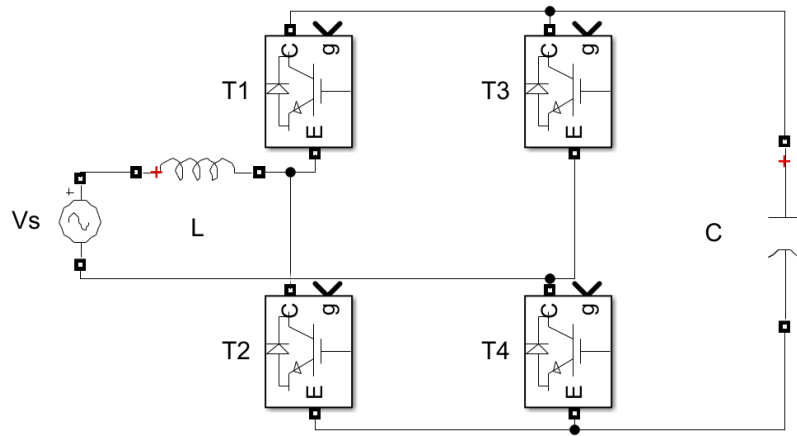


Figure 3.5: AC/DC power converter for the traction system

(as seen in figure 3.5) closes and the inductor's current increases as described by the following equation.

$$\Delta I_L = \frac{V_s}{L} \cdot t_{on} \quad (3.57)$$

From this equation it can be concluded that the current that passes through the inductor will vary significantly based on the instantaneous value of the AC voltage. This will lead the current that passes through the inductor to have an approximately sinusoidal shape.

When the transistor opens, the current stops passing by transistor 2 and passes through the diode of the transistor T1 in order to charge the capacitor. Since the voltage of the capacitor is higher than the voltage of the source, the current in the inductor will decrease its value until it reaches 0A. This variation in the current can be expressed by the expression:

$$\Delta I_L = \frac{V_s - V_C}{L} \cdot t_{off} \quad (3.58)$$

The charge variation on the capacitor, while the transistor two is open and current is flowing through the anti-parallel diode in transistor one, can be described as:

$$\Delta V = \frac{I_L}{C} \cdot t_{off} \quad (3.59)$$

Due to the sinusoidal aspect of the current in the coil, it is also expected that the voltage of the capacitor will oscillate at 100Hz, the frequency of the half wave of the sinusoidal source.

When the voltage of the sinusoidal source is negative the circuit will use the right arm of the converter to increase the current of the coil and subsequently charge the capacitor. The transistor four will close to increase the current of the coil and when it closes the current will flow by the diode of the transistor four, being stored in the capacitor and increasing its voltage.

Due to the oscillating nature of the input voltage, the current that passes through the coil will not always be above zero which will lead the converter to have a discontinuous current operation.

The system presented in [29] is similar to the micro grid being studied in this dissertation and, from there, the value of the DC link capacitor can be obtained as 9mF. Since in [29] only one motor is considered, the value used for this dissertation will be four times that to achieve similar operational conditions, meaning that the capacitor will have a capacity of 36mF.

For the inductor, it is intended that the LC filter has a cut-off frequency of 50Hz and, knowing that:

$$f_c = \frac{1}{2 \cdot \pi \cdot \sqrt{C \cdot L}} \Leftrightarrow L = \frac{1}{(2 \cdot \pi \cdot f_c)^2 \cdot C} \quad (3.60)$$

$$L = L = \frac{1}{(2 \cdot \pi \cdot 50)^2 \cdot 36 \cdot 10^{-3}} = 281.45 \mu H \quad (3.61)$$

3.4.2 AC/DC Converter Controller

In order to control the converter previously presented, it is necessary to generate PWM signals, with the appropriate duty-cycle, for the transistors two and four. Transistor two must only operate when the AC line has a positive value, remaining open at other times, and transistor four must operate when the AC line has a negative value, remaining open at all other times.

To achieve this goal a voltage feedback loop controller was implemented. This controller is made of three parts, the first is a standard PI controller that takes in the voltage error of the DC link and outputs a duty-cycle reference through the expression:

$$D = e \cdot \left(K_p + \frac{K_i}{s} \right) \quad (3.62)$$

For this implementation the value for the proportional and integral gains were as follows:

$$D = e \cdot \left(0.001 + \frac{0.01}{s} \right) \quad (3.63)$$

The second part of the controller selects which transistor should receive the PWM signal by measuring the instantaneous value of the 1500V AC voltage. The duty-cycle of each of the transistors, two and four, can be described by the equations that follow.

$$D_{T_2} = \begin{cases} D, & V_s(t) > 0; \\ 0, & V_s(t) \leq 0; \end{cases} \quad D_{T_4} = \begin{cases} D, & V_s(t) < 0; \\ 0, & V_s(t) \geq 0; \end{cases} \quad (3.64)$$

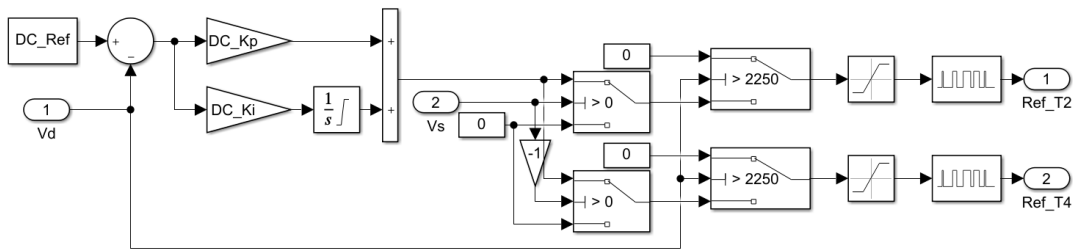


Figure 3.6: AC/DC converter controller implementation in Matlab/Simulink

For last the duty-cycles calculated are used as the input for PWM generators, that produce pulses at 1250Hz, and those signals are used to drive the gates of the transistors two and four.

This controller was implemented in the Matlab/Simulink model as can be seen in figure 3.6

3.4.3 DC/AC Inverter

The DC to AC inverter consists of a transistor three phase H bridge that converts the 2200V DC link voltage, created by the AC/DC converter, and outputs an AC current that is used to power an induction motor. This converter outputs a PWM voltage and the windings of the motor act as the filter so that an AC sinusoidal current is obtained.

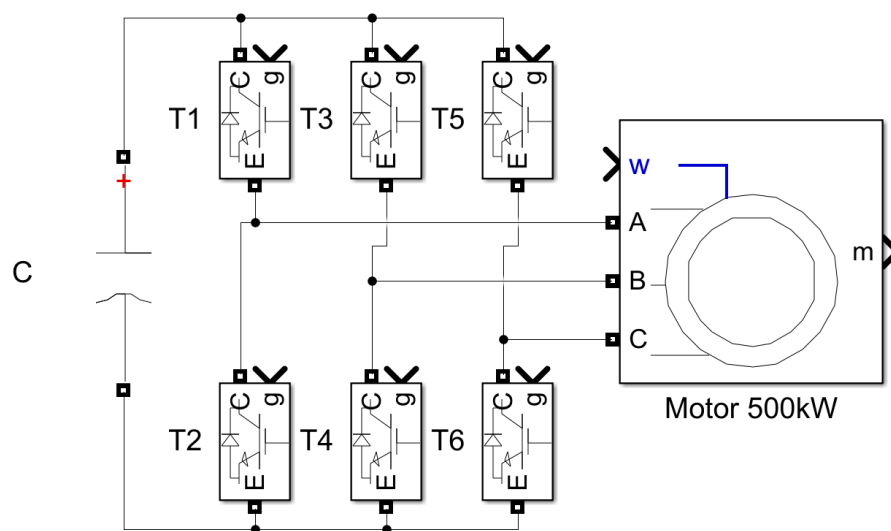


Figure 3.7: DC/AC Inverter powering 3 phase induction motor

To achieve the intended current waves that power the motor, the transistors in each arm switch in a complementary manner with a variable duty-cycle PWM. The PWM signals are generated with the SVPWM method that generates six signals, complementary two by two, that impose the output currents with a 120° difference between them.

The 4000 series train is powered by 500kW, three phase induction motors. In order to simulate an adequate motor the internal parameters, required by the software Matlab/Simulink, had to be defined. Based on multiple existing models of three phase induction motors on Simulink, these parameters were estimated and the ones present in table 3.3 were used during the whole dissertation work.

To find the motor's power factor a simulation was done where the motor was connected to sinusoidal voltage sources with all the motor nominal parameters. From the acquisition of the current and voltage values of the three phases of the motor it was possible to calculate the active and reactive power of the motor and with it, the power factor. The implementation used to calculate the power factor can be seen in the image below.

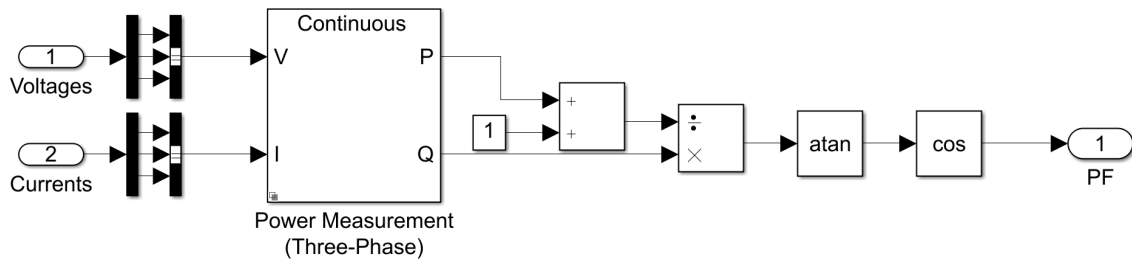


Figure 3.8: Simulink block used to calculate the power factor of the motor

From this simulation it was found that the value of the power factor of these motors is 73.43%. The phase currents from this simulation were also scoped and the nominal value of the phase current was measured as 374.4A RMS.

IM Parameter	Value	Unit
Power	500	kW
Frequency	50	Hz
Voltage	1100	V
Pole Pairs	2	
Stator Resistance	41.693	ohm(Ω)
Rotor Resistance	25.688	ohm(Ω)
Stator Inductance	376.579	μ H
Rotor Inductance	376.579	μ H
Mutual Inductance	8.3	mH
Rotor Type	Squirrel Cage	

Table 3.3: Three phase induction motor parameters

With these values, the efficiency of the motor can be calculated as:

$$\rho_{100\%} = \frac{P}{\sqrt{3} \cdot V \cdot I \cdot PF} \quad (3.65)$$

Replacing into the formula by the known values, it becomes:

$$\rho_{100\%} = \frac{500000}{\sqrt{3} \cdot 1100 \cdot 374.4 \cdot 0.7343} = 95.46\% \quad (3.66)$$

On the Simulink model, the induction motor is represented by an asynchronous machine that has as an input the rotational velocity of the rotor, given by the output provided by the block present in figure 3.3, divided by the radius of the wheels to convert linear velocity to rotational velocity. The other inputs present in the motor's model correspond to the power lines of each phase that have their origin in the three arms of the inverter. As the output the motor provides the value of the torque that is being produced, which is then converted to force by the means of equation 3.17. This force value is used as the input of the block that simulates the train's physical behaviour, which then uses this value to update the velocity at which the train is travelling.

3.4.4 DC/AC Inverter and Motor Control

The goal of the DC/AC Inverter is to generate the correct gate signals for the six transistors in order to obtain the desired behaviour from the motor and, consequently, the train. To achieve this, there was the necessity to implement a controller in five parts, a flux reference controller, a torque reference controller, a q axis controller, a d axis controller and the SVPWM gate signal generator.

This controller uses a FOC approach where the stator voltages and currents are measured and, with those values, the instantaneous flux and torque values of the motor are calculated. Since the flux of an induction motor is representative of its d axis current in a dq referential of the current that pass through the motor, and the torque is representative of the q axis current, these values can be used to generate d and q references for the SVPWM generator block. This approach enables a precise control of the flux and torque of the motor at all instants, guaranteeing that the system has the desired behaviour.

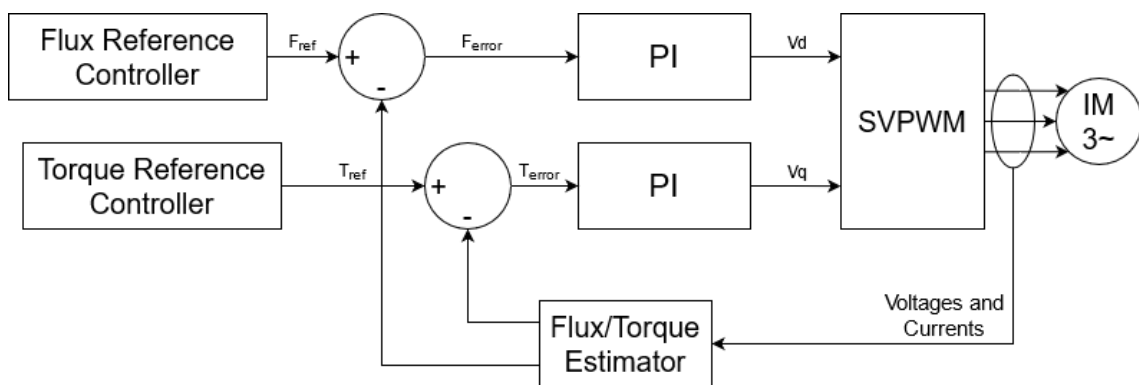


Figure 3.9: Implemented FOC controller block diagram

Due to the multiple conditions under which the train must operate, there are four major operating modes that can be defined for the train. These modes define how the propulsion system must act at a given moment and they can be described as follows.

- **Acceleration** - the motors are required to produce the maximum torque, as explained in [3.2.3.1](#)
- **Cruising** - the controller must guarantee that the train maintains a constant specified velocity
- **Coasting** - the motors must stop producing work and the train will travel only relying on inertia, reducing its speed over time due to the drag and friction forces applied.
- **Deceleration** - The motors must produce negative torque to reduce the speed of the train, just like with the acceleration, it is optimal to produce the maximum (in absolute value) torque possible to maximize efficiency.

To generate a reference value for the flux of the motor, the rotational speed of the rotor must be taken into account, since the motor has to work in a field weakening mode after it achieves its

synchronous speed (when the train travels at 19.0476m/s). The proposed implementation follows a common field weakening technique that reduces the flux value as an inverse proportion of the rotor frequency.

By performing some simulation tests to the motor, it was measured that the flux produced by the motor while working at nominal conditions is 2.8077Wb.

The model implemented in Matlab/Simulink to generate the flux reference value is displayed in figure 3.10.

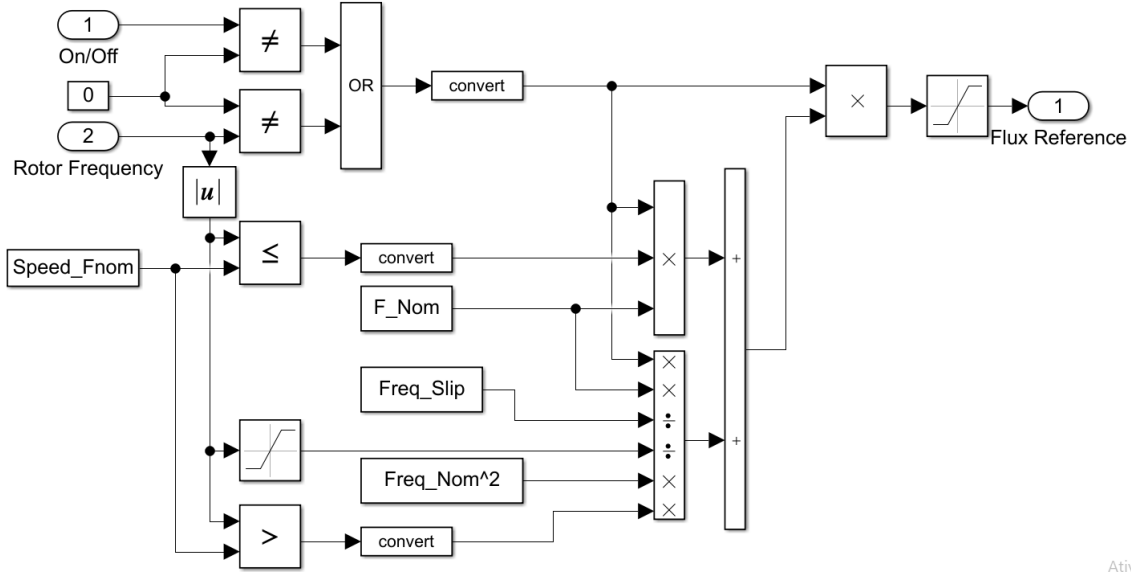


Figure 3.10: Implemented Flux Reference Controller

For the coasting mode, where the motor does not need to produce any torque, the reference given to the d axis current controller is 0, and this will lead to the motor being turned off. For all three other operation modes the reference given to the motor from zero hertz up until the rotor achieves the synchronism frequency is the nominal flux.

From there up until the motor reaches its maximum speed, when the train travels at 220km/h, the flux reference given to the motor decreases proportionally with the speed increase. The reference value produced by this controller when the motor is in a field weakening region is also affected by a correction factor to take into account the slip of the motor. The controller presented in figure 3.10 can be described by the next equations.

$$F_{ref} = \begin{cases} F_{Nom}, & Freq_{rotor} < F_{synchronism}; \\ \frac{F_{Nom} \cdot Freq_{Nom}^2}{Freq_{rotor} \cdot Freq_{Slip}}, & Freq_{rotor} \geq F_{synchronism}; \end{cases} \quad (3.67)$$

To generate a d axis voltage reference, the estimated flux value is compared with the reference generated by the Flux Reference Controller and the error is obtained. This error value is then normalized, by multiplying it by $\frac{1}{F_{Nom}}$, and then that value is used as the input for a PI controller that outputs the V_d reference.

The output of this PI controller is limited on the upper side to 1 in order to prevent the PI controller to provide a reference V_d that is higher than the range accepted by the SVPWM generator block. The output of the controller is also limited on the lower side to 0 since the flux of the motor, to guarantee a correct operation while producing positive and negative values of torque, has to be positive. This output can be described by the equation:

$$V_{dref} = F_{error} \cdot K \cdot \left(K_p + \frac{K_i}{s} \right) \quad (3.68)$$

By an heuristic manner, values for the integral and proportional gains were defined and, when replaced in equation 3.68 the following is obtained.

$$V_{dref} = \frac{F_{error} \cdot \left(0.01 + \frac{0.3}{s} \right)}{2.8077} \quad (3.69)$$

The Matlab/Simulink implementation of this controller is the one portrayed in figure 3.11.

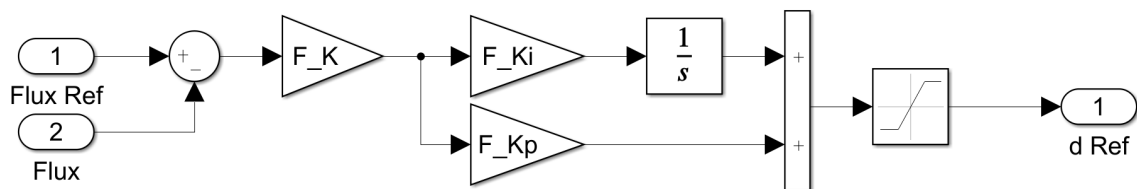


Figure 3.11: Implemented d axis controller

To control the torque produced by the motor, which is directly tied with the value of the quadrature current of the motor in a dq referential, a torque reference controller was designed to output a reference value for the motor's torque. Due to the many operation modes of the train, this controller was required to take into consideration many situations that can occur while the train is moving.

The controller starts by selecting, based on the current velocity and the velocity reference, which of the four modes it should consider. This task is done by means of a state machine that has for inputs the current mode, the velocity error, the current velocity of the train, the variation between the current and the previous speed references provided to the controller and a boolean value that indicates if the train should be on or off. This boolean signal is active when the train is intended to enter the coasting mode of operation or, if the train is not moving, to indicate that the train should remain stopped.

This state machine is initiated in a default mode where the train is completely stopped, when the reference value provided for the speed changes from zero meters per second to any positive value (it is assumed that the train can only have positive values of velocity), the mode at which the controller is set changes to enable an acceleration event. From here the train can change to either of the three remaining modes. If the train achieves the reference speed, it changes to the coasting mode, maintaining the speed constant. In case the train receives a speed reference with

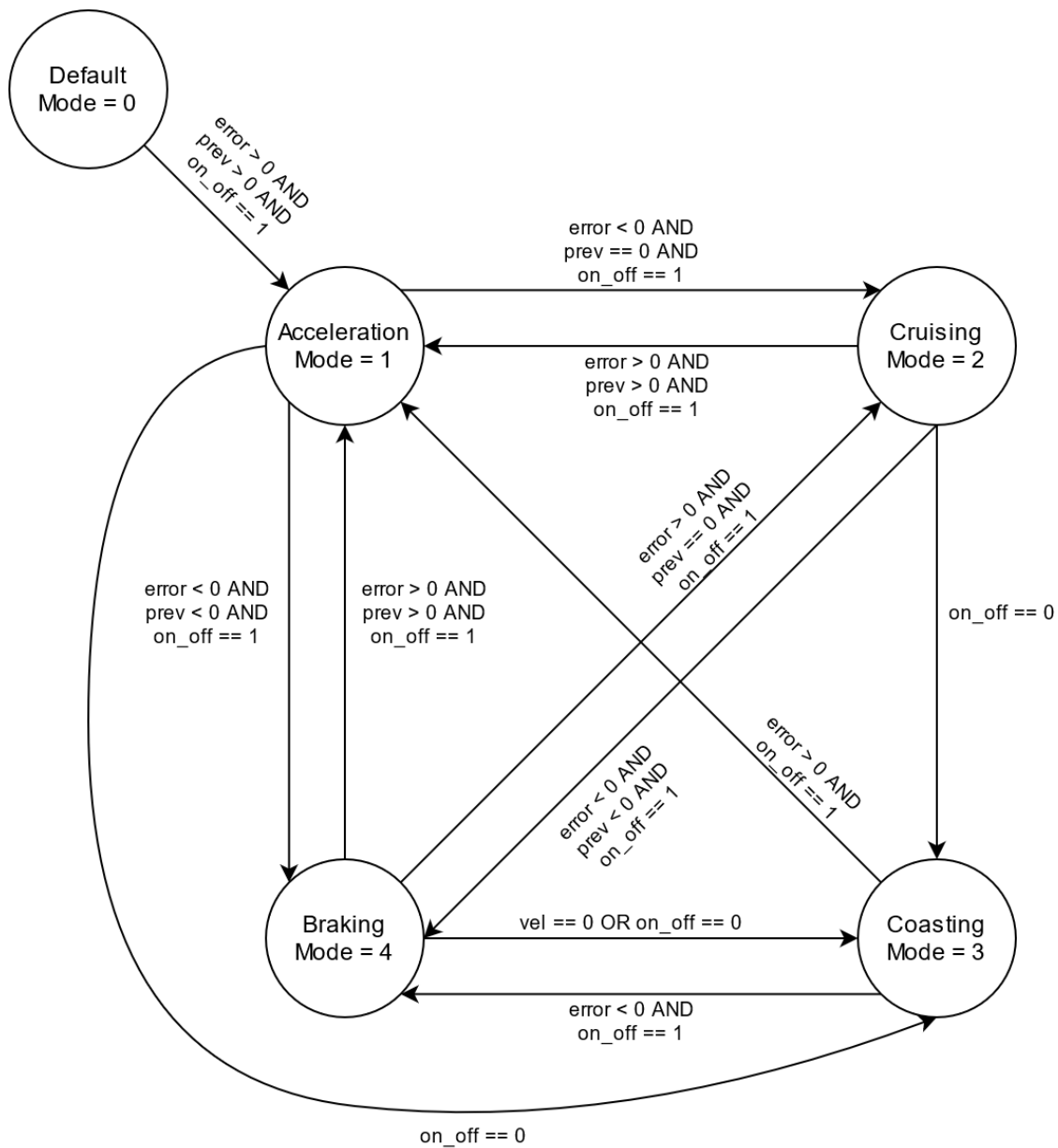


Figure 3.12: Operation mode Selector state machine

a value below the current speed of the train, it changes to the braking mode. If the value of the boolean signal that indicates if the engines should be on or off becomes zero, the train switches to the coasting mode.

When the system is in cruising mode at a fixed speed, if the speed reference is changed one of two things can happen. If the new speed reference is higher than the previous, the controller switches to the acceleration mode, in case the new reference is lower than the cruising speed of the train, the system transitions to the braking mode. If the boolean signal indicates that the engines should be off, the controller switches to the coasting mode.

While in braking mode, just like in the previously described modes, if the boolean signal is

zero, the controller enters the coasting mode, although, unlike the other modes, while the train is braking if the train stops the train also enters coasting mode. If the reference speed changes, whilst the train is braking, to a higher value than the speed of the train, the controller changes from the braking to the acceleration state. In case that, during the deceleration process, the train achieves the reference speed, the output of the state machine becomes the cruising mode.

In the situation where the train is coasting, if the boolean signal indicates that the motors should produce torque, there are two possible situations that can occur. If the reference speed is higher than the travelling speed the state machine's output becomes the acceleration mode, otherwise the train enters a braking event.

Once the operating mode is selected, the behaviour of the controller varies depending on what is expected for it to do. When the selected mode is the acceleration one, the reference torque generated by the controller increases with a rate per second of twice the nominal torque. In this sub-controller, an integral controller is also summed to the ramp signal, when the torque of the motors approaches its nominal value. This is done to reduce the time it takes the motor to achieve its nominal torque. The implementation developed in Matlab/Simulink of this controller is present in figure 3.13.

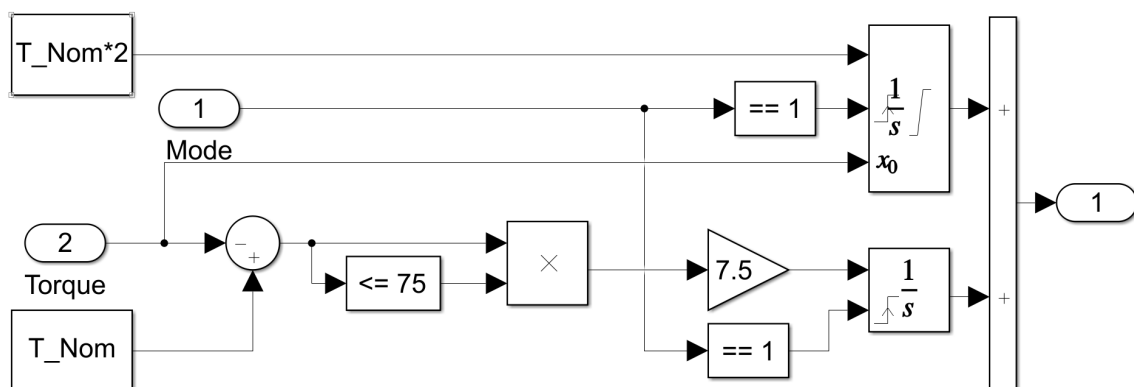


Figure 3.13: Acceleration sub-controller

When the train's selected mode of operation is cruising, the torque reference is generated in two steps. Firstly, based on equation 3.15, the torque required to maintain the desired speed is calculated and forwarded to another sub-controller. This sub-controller proceeds to change the torque reference by means of a ramp, starting at the torque value the motor is producing until the reference matches the value calculated for the intended cruising speed. Since the terrain and weather conditions may present small variations, the output of a PI controller is added to this reference to compensate said variations. This allows the train to maintain the cruising speed consistent throughout the all time when it is operating in cruising mode. The ramp controller and the PI controller implemented in the software Matlab/Simulink can be seen as follows in figures 3.14 and 3.15, respectively.

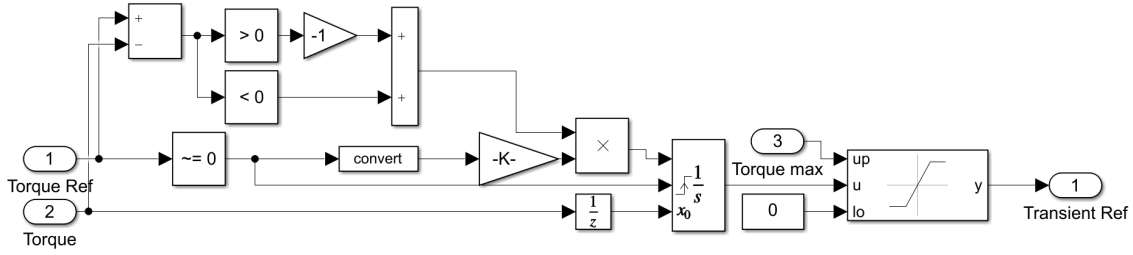


Figure 3.14: Cruising sub-controller

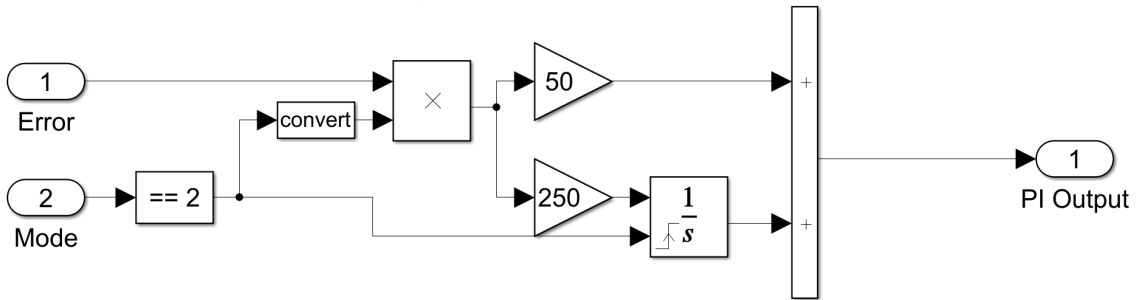


Figure 3.15: Cruising torque reference compensation PI controller

For the braking mode of operation, the controller generates a reference corresponding to the maximum possible braking torque, which is obtained by:

$$T_{max_{brake}} = 0.79 \cdot T_{m-0} = 0.79 \cdot 3226.86 = 2549.22N \cdot m \quad (3.70)$$

In order to guarantee that the torque references generated by this controller never exceed the maximum values possible for a given speed, a block that defines the saturation limits for the reference was created. This limiter starts by calculating the maximum torque available for a given motor frequency by means of the equation 3.12.

If the frequency of the motor is higher than its synchronism frequency, the motor is in a field weakening region and thus its direct current in the rotating dq reference frame decreases due to the flux reduction. This reduction enables the controller to increase the torque higher than the value defined by equation 3.12, by increasing the quadrature current, as long as the motor's I_s current remains under its maximum value. From the nominal current of the motor, measured through a scope in Matlab/Simulink, and using equation 2.10 this value can be calculated.

$$I_s = \sqrt{2} \cdot 374.4 = 529.48A \quad (3.71)$$

The controller implemented to calculate the allowed torque increase calculates the motor's instantaneous I_s current from the measured direct and quadrature currents by means of equation

2.10. If the frequency of the motor is higher than the synchronism one, the controller integrates the error between the nominal I_s and the measured one and with an integral controller generates an offset that is added to the value calculated by applying equation 3.12. The implementation of this controller in Matlab/Simulink is illustrated in figure 3.16.

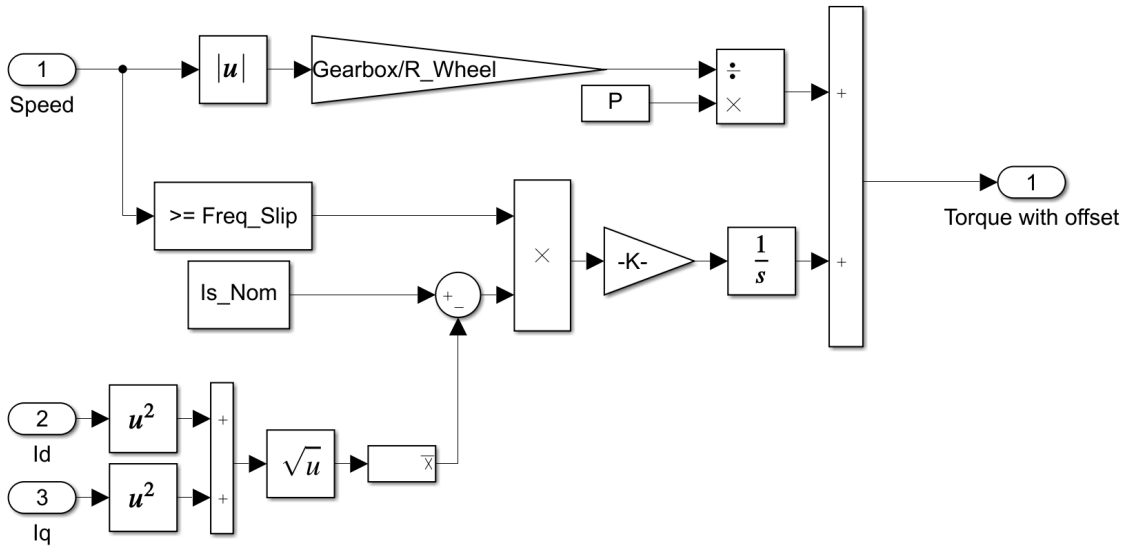


Figure 3.16: Maximum torque reference offset controller

The complete implementation of the torque reference controller can be seen in appendix B.1.

After generating a reference for the motor's torque, this value is processed in a similar manner as the flux of the motor. The difference between the reference and the estimated torque value is passed forward as an error signal that is then normalized to fit a scale between -1 and 1. The normalized error is used as the input for a PI controller that generates a quadrature reference for the voltage signal that will be used by the SVPWM block. Just like the output of the controller from figure 3.11, the output of this one is also limited between -1 and 1 to prevent over-modulation from occurring in the SVPWM block.

The output of this controller can be described as:

$$V_{qref} = T_{error} \cdot K \cdot \left(K_p + \frac{K_i}{s} \right) \quad (3.72)$$

$$V_{qref} = \frac{T_{error} \cdot \left(0.5 + \frac{30}{s} \right)}{3226.86} \quad (3.73)$$

This controller's implementation is the one present in figure 3.17.

After calculating both the direct and quadrature voltage references, these two signals are passed forward in order to generate the pulses for all six transistors that feed the motor. Since the block present in Matlab/Simulink that implements the SVPWM function requires as inputs a

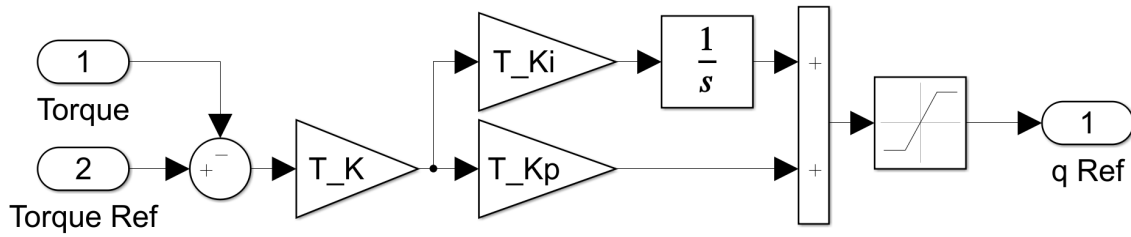


Figure 3.17: Implemented q axis controller

magnitude and an angle signals, the dq references must be converted to their alpha beta equivalents with equation 2.11.

To transform the alpha and beta references into a magnitude and angle references the equations that follow can be implemented, respectively.

$$|U| = \sqrt{V_{\alpha}^2 + V_{\beta}^2} \quad (3.74)$$

$$\angle U = \arctan \frac{V_{\beta}}{V_{\alpha}} \quad (3.75)$$

From these two references the SVPWM block generates the six pulses, complementary two by two, that switch the transistors that power the motor. This implementation can be observed in figure 3.18.

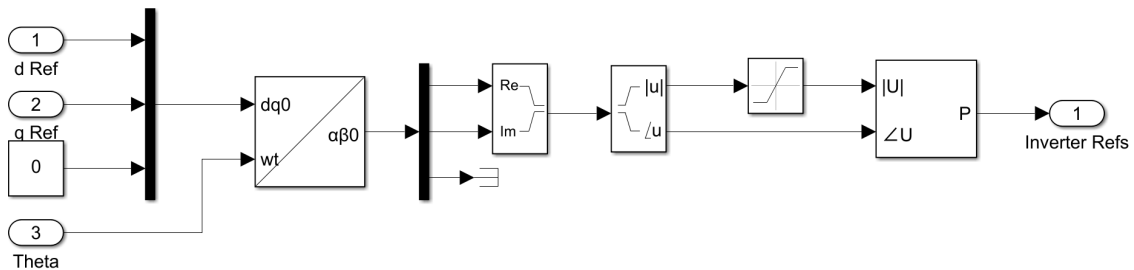


Figure 3.18: SVPWM motor controller Matlab/Simulink implementation

The controllers described are dependent of the value of either the flux or the torque that the motor is producing at any given moment. These two values are estimated based on the voltages and currents on the motor using the equations 2.15 and 2.18.

To calculate the dq currents, the angle of the flux in the air gap is required and the equation 2.19 was implemented in order to obtain that value which is then provided to the Park transform block.

The implementation done in Matlab/Simulink of the torque and flux estimator is the one present in figure 3.19.

The complete electrical system model of the train, implemented in Matlab/Simulink can be analysed in B.2.

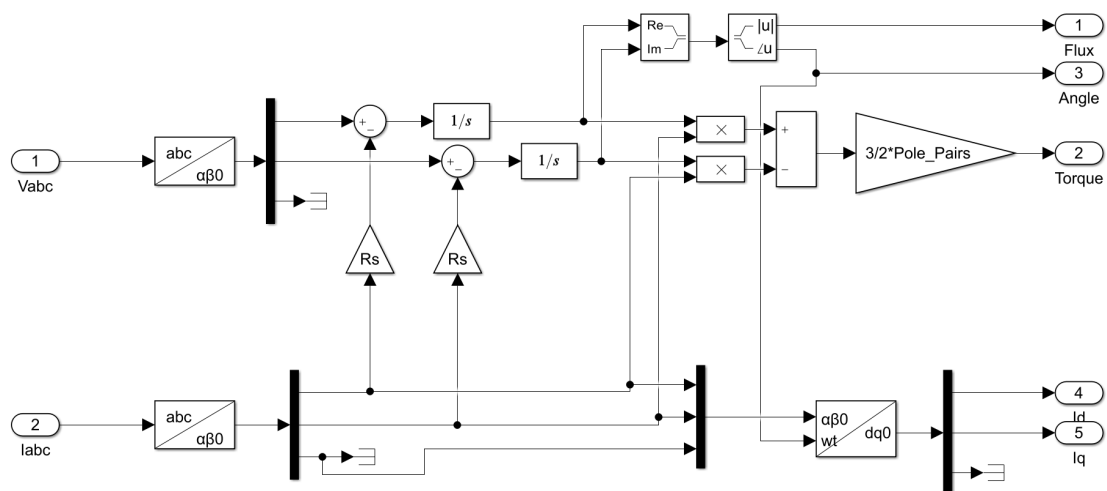


Figure 3.19: Torque and Flux estimator implementation in Matlab/Simulink

3.5 Auxiliary Systems

To power all the equipment that exist on the train and guarantee a comfortable and trouble free voyage for the passengers, such as the air-conditioning units, the lights and power sockets, it is necessary to create a three phase 400V (phase-phase) grid inside the train.

The converters required to create this grid are very similar to the ones used to power the motors since both systems have the goal of powering three phase AC systems. The AC/DC converter generates a 1500V DC link from a 600V AC source that originates on the transformer connected to the catenary. Since the power requirements for this converter are lower than the ones from the traction system, the capacitor for this converter has a capacity of 25mF and the inductor has a value of $65\mu H$. The control used for this converter is the same one used for the AC/DC converter in the traction system, but the reference DC voltage is changed from 2200V to 1500V.

The 1500V DC link is then used to feed an inverter that generates the three phases with a 120 degree phase between them. Unlike the inverter used for the traction system, the one that powers the auxiliary systems requires a filter to output the intended voltage wave forms. This happens because on the traction system the motor itself acted as a filter.

Due to the nature of the system, this converter must operate as a grid forming converter and thus maintain the voltages constant during load variations. To achieve this goal, the controller creates three sinusoidal voltage references and transforms them to a dq rotating frame, by using the method from equation 2.12. The reference voltages are compared with the dq voltages, obtain by transforming the measured three phase voltages, and the error signal is forwarded to a PI controller that generates current dq references.

The dq current references are then compared to the currents obtained by applying the equation 2.12 to the measured currents and the error signal is used to generate the dq references that can be used to generate the pulses that drive the transistors from the inverter. Due to the specificities of

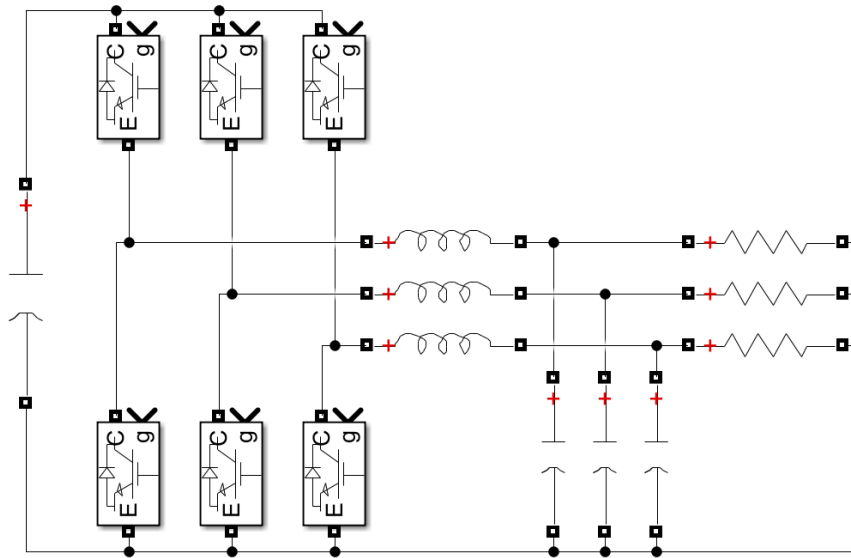


Figure 3.20: AC/DC power converter for the auxiliary systems

the Matlab/Simulink SVPWM blocks, the dq references are converted to the alpha beta stationary frame of reference to serve as inputs of the SVPWM block, that outputs the six gate signals.

The angle required for all the direct and inverse dq transformations of this controller is calculated by integrating the value of the frequency that is intended for the output voltages.

The implementation of the controller in the Matlab/Simulink environment can be analysed in the figure below:

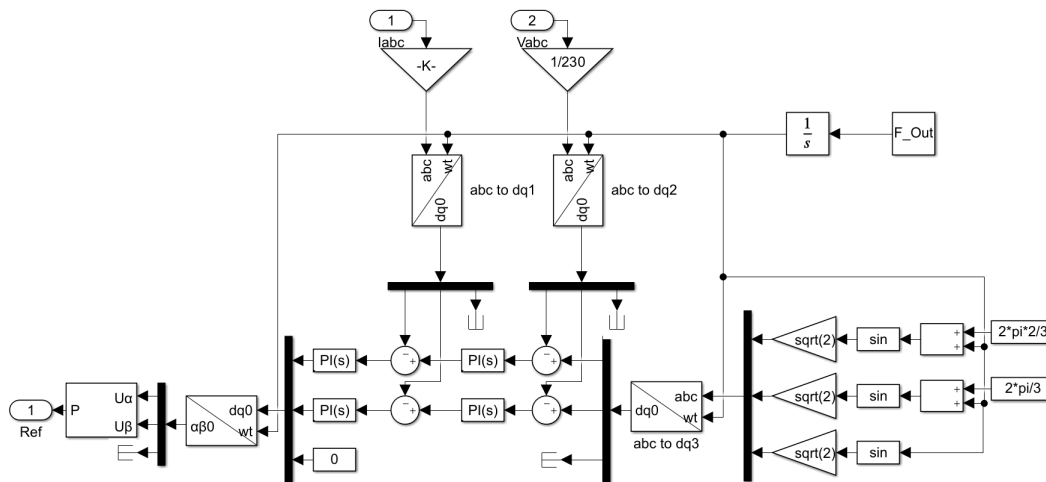


Figure 3.21: DC/AC inverter grid forming controller implementation in Matlab/Simulink

The complete schematic of the electrical implementation of the auxiliary systems, in Matlab/Simulink, is presented in figure 3.22.

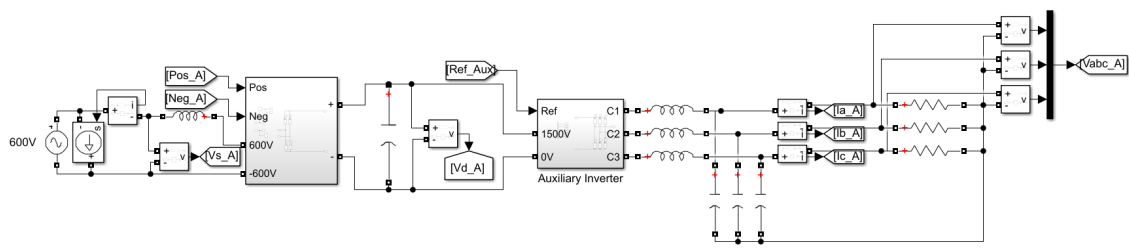


Figure 3.22: Electrical model of the traction system implemented in Matlab/Simulink

3.6 Conclusions

Throughout this chapter, the process used to create an accurate and complete model of a 4000 series train was presented. The physical equations that describe the movement of the train across all its operational modes were explained. The power converters required to power all the train converters were also discussed as well as the converters required to drive them along with their implementations in the simulation environment.

Chapter 4

Photovoltaic Production System

4.1 Summary

A six carriage train, such as the series 4000, has a large area on the roof that is currently being wasted and with the implementation of a photovoltaic production system, can be used to reduce the grid power requirements from the train. This chapter will discuss the solar capability of the roof of the train and its distributions by the different carriages, along with the array configuration for each of the carriages. Then the converter, required to deliver the generated power to the train, and its controller will be discussed and their implementation in the simulation environment of Matlab/Simulink will be presented.

4.2 Array Configurations

The carriages of the series 4000 train have a different roof profile due to the existence of some crucial components on there, such as the pantographs and the air-conditioning units. To determine the capacity of solar panels that is possible to install in each carriage three things are required to be determined:

- The width of each carriage;
- The length of each carriage that is unobstructed by equipment;
- The size and power output of each solar panel.

From the diagrams from [2], shown in image 4.1, it is possible to determine, with the help of some basic image software, that the width of the roof of the train is 260cm.

To determine the areas where solar panels can be fit, the image from appendix C.1, was studied and it was determined that there are four different roof profiles across the six carriages.

- The conductor carriages (corresponding to the BAS and BAN carriages in the image from appendix C.1), that have an available area of 20.45m by 2.60m each;

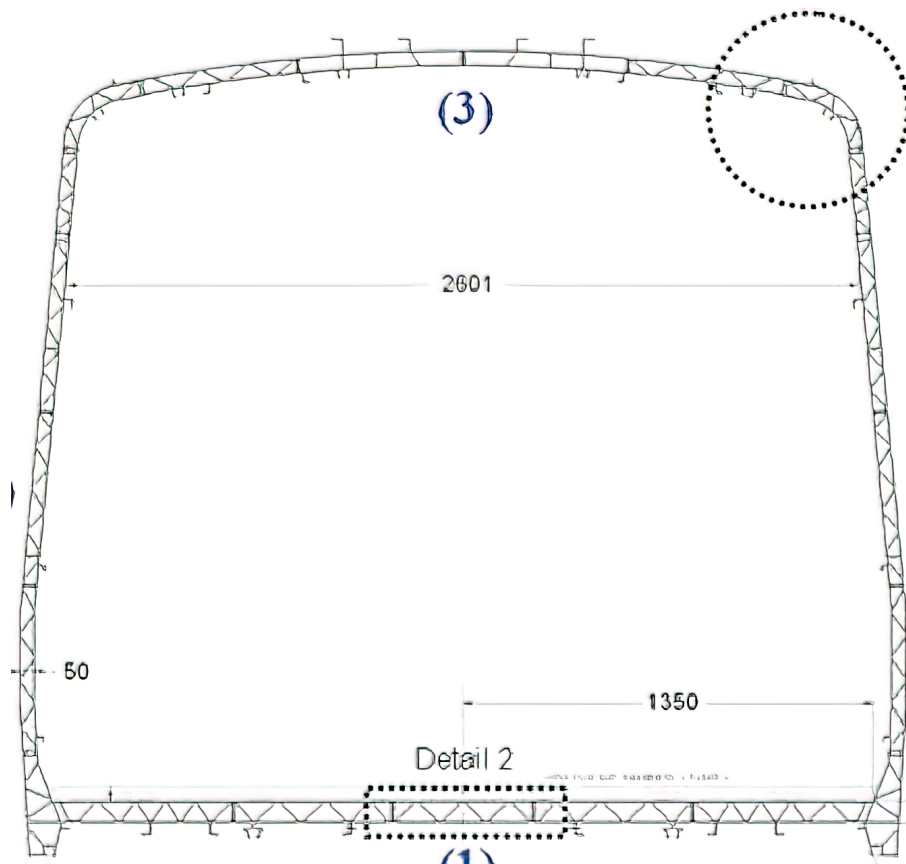


Figure 4.1: Cross section of a carriage from a series 4000 train [2]

- The middle carriages that have no equipment on the roof (corresponding to the BBS and BBN carriages in the image from appendix C.1), that have an area of 25.00m by 2.60m each;
- The carriage that has the air-conditioning unit and the pantograph in adjacent places (corresponding to the RNH carriage in the image from appendix C.1), that has two separate areas with 17.87m by 2.60m and 1.47m by 2.60m;
- The carriage that has the air-conditioning unit and the pantograph in separate places (corresponding to the RNB carriage in the image from appendix C.1), that has three separate areas with 1.68m by 2.60m, 7.33m by 2.60m and 10.47m by 2.60m.

From a market research, it was determined that a normal size for flexible solar panels is 1.219m by 0.549m for a 100W solar panel. From these measurements, the number of solar panels for each carriage can be determined. The optimal layout of panels, to reduce empty space, is to lay two panels across the width of the carriage, in order to leave empty just 16cm of the width of the carriage. From this, and based on the measurements presented, each carriage type can determine the number of panels and produce the maximum power as indicated in table 4.1.

On each carriage the panels will be connected in two parallel strings, each with equal number of panels, this will be done so that the voltage of each string is not too low when compared to the 1500V of the DC link of the auxiliary systems where the solar generated power will be injected in the train's grid.

Carriage	Number of panels	Installed Power
BAS and BAN	74 each	7400W each
BBS and BBN	90 each	9000W each
RNH	68	6800W
RNB	70	7000W

Table 4.1: Number of panels and installed power for each type of carriage

The solar panel parameters selected [30] for the simulation as the following electrical characteristics.

Specification	Value	Unit
Maximum Power	100	W
Number of cells	36	
Open circuit Voltage	22.5	V
Short-circuit current	5.75	A
Voltage at MPP	18.9	V
Current at MPP	5.29	A

Table 4.2: Solar panel characteristics

4.3 DC/DC converter

To minimize conduction losses and simplify the installation, each carriage will be equipped with a converter that feeds the power, generated by the panels on its roof, to the 1500V DC link. On the roof of each carriage, the panels will be divided in two strings, this will guarantee an output voltage high enough to achieve an efficient DC/DC conversion. Since different carriages have a different number of solar panels, the DC voltage of each carriage will be different. These voltages are as follows in table 4.3.

Carriage	Voltage
BAS and BAN	699.3V
BBS and BBN	850.5V
RNH	642.6V
RNB	661.5V

Table 4.3: DC voltage of the panel strings for each carriage type

Since the output voltage of the panel strings is lower than the one from the DC link, a boost converter will be used to feed the power from the panels to the DC link and, subsequently, the auxiliary systems of the train. This type of converter has the structure present in figure 4.2.

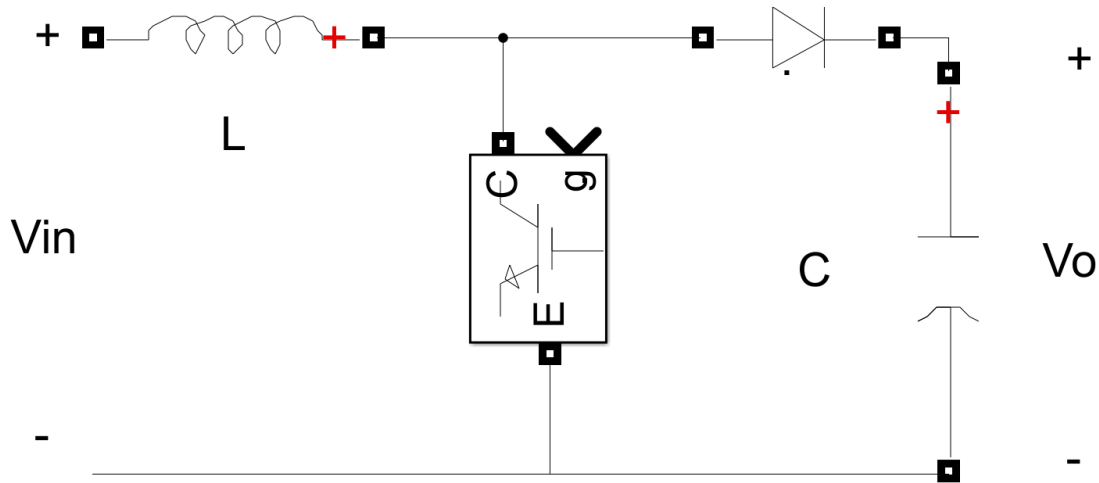


Figure 4.2: DC/DC Boost converter structure

While it operates, the converter can have two states (in a continuous current mode of operation), when the transistor is open and when it is closed. When the transistor is closed, there is a positive voltage applied to the coil and its current increases. When the transistor opens, the current flows through the diode to the capacitor charging it. At this time the voltage on the coil is negative and the current decreases. The transfer function of this converter is:

$$\frac{V_o}{V_{in}} = \frac{1}{1 - D} \quad (4.1)$$

Considering that, at the voltage of the panel strings is known, when they operate at the maximum power point, by rearranging equation 4.1, the expected duty-cycles for the converter of each carriage can be determined.

$$D = 1 - \frac{V_{in}}{V_o} \quad (4.2)$$

Applying equation 4.2 to the values from table 4.3, the expected duty-cycles for the converters in each carriage are determined as:

Carriage	Duty-cycle
BAS and BAN	0.5338
BBS and BBN	0.4330
RNH	0.5716
RNB	0.5590

Table 4.4: Duty-cycles of the DC/DC boost converters for each carriage type

The ripple of the current that goes through the coil can be expressed as:

$$\Delta I_L = \frac{V_{in}}{L} \cdot t_{on} \tag{4.3}$$

For the implementation of these converters in the Matlab/Simulink environment, a block that implements the complete strings of the panels based on the characteristics from table 4.2 and the number of panels in series and parallel. This block generates characteristic curves for the panel for different irradiance levels, the ones from the panel used are displayed in figure 4.3.

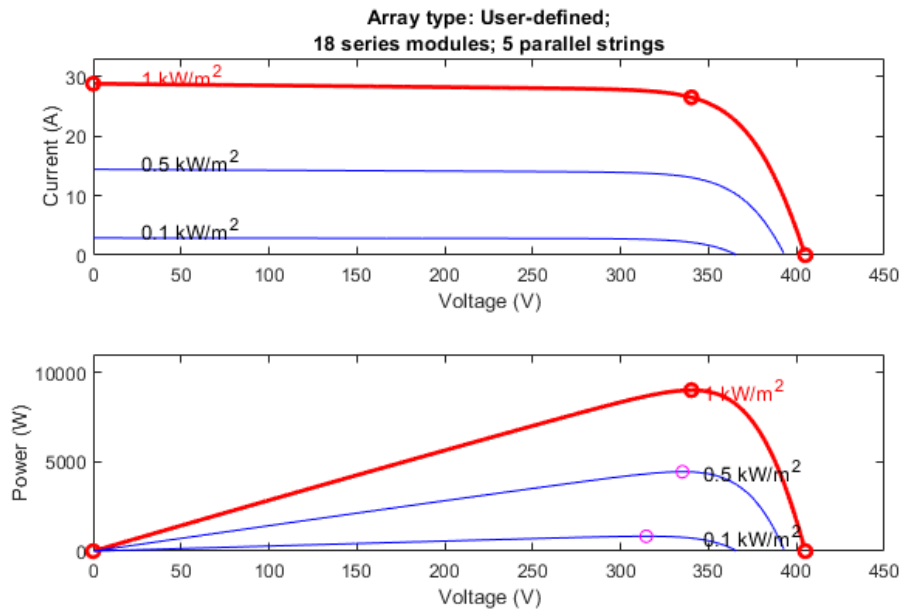


Figure 4.3: Solar panel I-V characteristic curve (top), Solar panel P-V characteristic curve (bottom)

For this specific implementation, the capacitor of the DC/DC boost converter is the capacitor from the DC link. The complete implementation of one of these converters and its solar panel array in Matlab/Simulink can be analysed below.

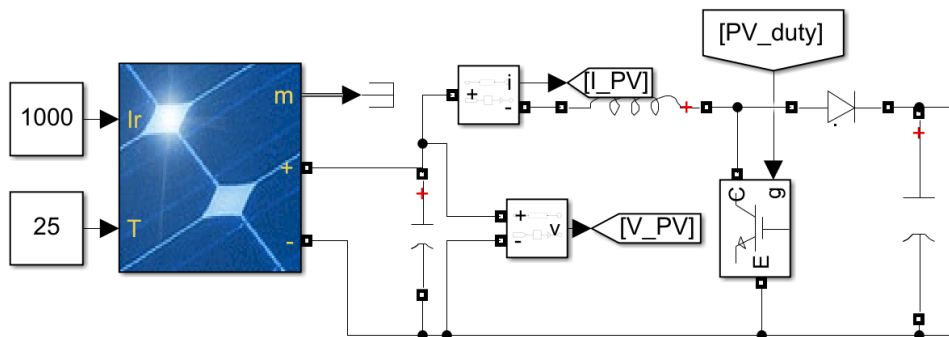


Figure 4.4: DC/DC Boost converter and solar array implementation in Matlab/Simulink

4.4 DC/DC converter controller (MPPT)

The main goal of the controller of this converter is to maintain the solar panels on their ideal operating point to produce the maximum power possible at any given time. Such a controller is called a maximum power point tracking controller and, for this application, its behaviour is conditioned by the measured voltage and current of each array of panels.

For the implementation in this dissertation, the MPPT method selected was the Perturb and Observe one. This control strategy begins by acquiring the voltage and current of the panel array and with these values the power output is calculated. The calculated power output is then compared to the previous power value and the voltage value is compared with the previous voltage value. If the power and voltage variations are both positive or both negative, the reference of the controller must be increased, if one of the variations is positive and the other negative the reference reference must be decreased. This control structure can be better shown by the graph below.

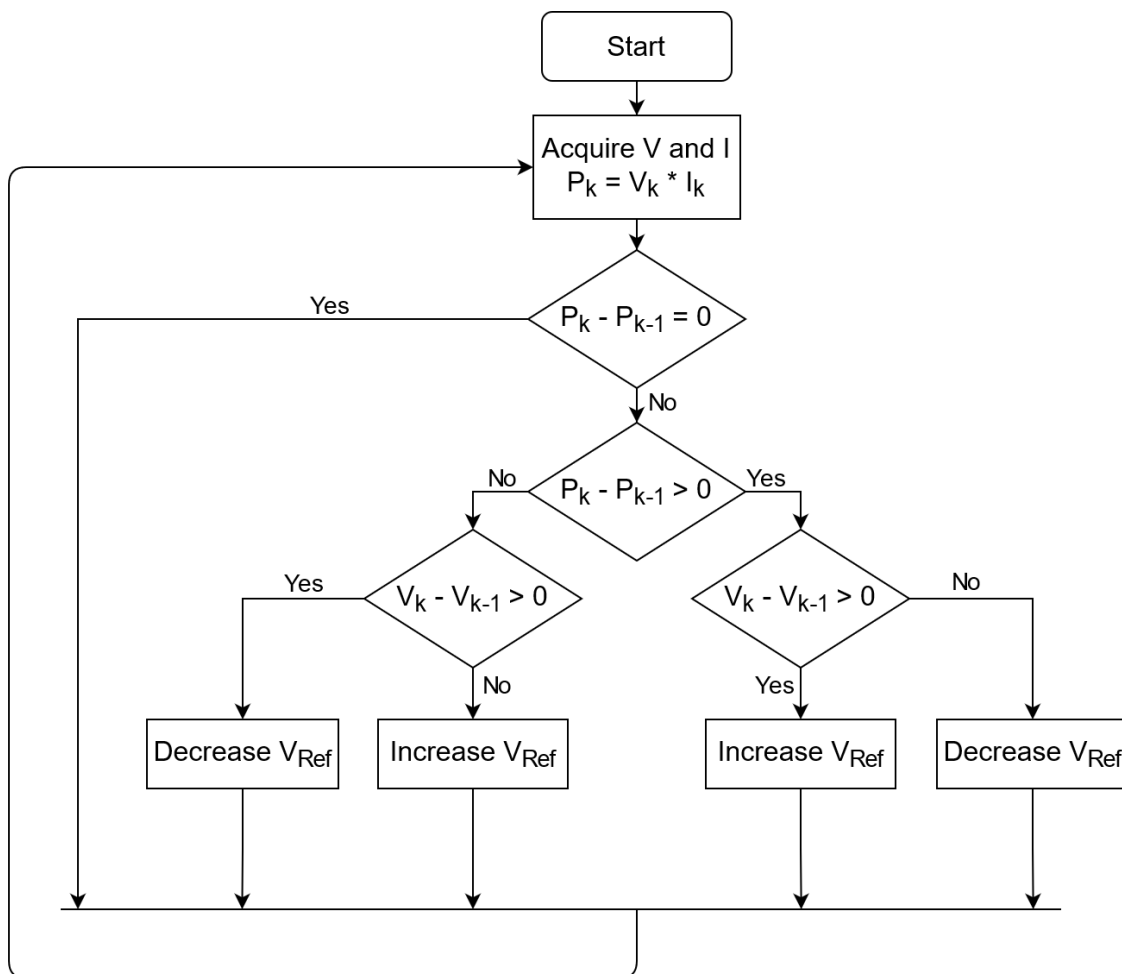


Figure 4.5: MPPT Perturb and Observe diagram

For ease of implementation, this control structure can be simplified and written as:

$$V_{ref} = \begin{cases} V_{Ref} + \Delta V_{Ref}, & \Delta P \cdot \Delta V > 0; \\ V_{Ref} - \Delta V_{Ref}, & \Delta P \cdot \Delta V < 0; \end{cases} \quad (4.4)$$

For the implementation of this controller in Matlab/Simulink, the equations from 4.4 were implemented. The controller's voltage and current signals are sampled with a period of 10ms. At initialization the controller sets a reference duty-cycle corresponding to the ones calculated for table 4.4. To avoid excessive commutation related to the ripple from the voltage and current signals, these signals are filtered and a commutation only occurs if the product of the power variation with the voltage variation has an absolute value above 0.5. The duty-cycle reference passes through a saturation block to prevent it from going outside the interval [0,1], and that reference is used as the input of the PWM block, whose pulses are used to drive the transistor of the converter.

The diagram implementation in Matlab/Simulink can be analysed in D.1.

Chapter 5

Energy Storage System

5.1 Summary

Electric braking allows for significant saving but, the energy must be stored somewhere so that it can be used later when needed. This chapter will be dedicated to size and compare the two most viable solutions for an energy storage system of this dimension, lithium ion batteries and super capacitors, and to describe the converter and controller designed to charge and discharge the OESS. For last the implementation in the Matlab/Simulink environment of this system will be presented.

5.2 Comparison

To size an ESS, there are two crucial parameters that must be taken into account, the capacity required to store all the energy that will be regenerated and the peak power of the regenerated energy.

The maximum energy that can be regenerated during a braking event, corresponds to the kinetic energy the train has at the beginning of that event. This sizing approach will consider that all the kinetic energy can be saved and that there are no losses due to resistive forces acting on the train. The system will be slightly oversized, but due to the degradation that occurs on storage devices across time, this will safeguard the integrity of the system for a longer period of time.

The maximum kinetic energy that the train can have occurs when it is travelling at its maximum velocity, and it can be described as the following equation:

$$E = \frac{1}{2} \cdot m \cdot v^2 \quad (5.1)$$

Replacing in this equation the variable by their respective numerical value, mentioned in 3.2, it becomes:

$$E = \frac{1}{2} \cdot 298300 \cdot 61.11^2 = 556.99MJ \quad (5.2)$$

The capacity of storage devices is measured in kWh, from equation 5.3 the value obtained in Joule can be converted to kWh.

$$Capacity = \frac{E}{3600 \cdot 10^3} = 154.72kWh \quad (5.3)$$

The maximum power being regenerated at a given time occurs at any speed equal or greater than the synchronism speed. In this speed range the power regenerated from braking will be 79% of the motors nominal power, since this is the relation between the maximum braking force and the maximum traction force.

$$P_{B_{max}} = 0.79 \cdot 4000000 = 3.16MW \quad (5.4)$$

Due to their nature, lithium ion batteries, unlike supercapacitors, have a very limited charge rate. With current technology allowing a maximum charge rate of 3C, the minimum capacity of the battery, that is able to accept the high power requirements can be calculated.

$$C_{battery} = \frac{P_{B_{max}}}{3} = \frac{3.16 \cdot 10^6}{3} = 1.053MWh \quad (5.5)$$

On the other hand, an OESS solution based on supercapacitors only requires the 154.72kWh capacity because they are able to be charge very high rates.

Considering the current price premium, per kWh, of five times of supercapacitors over lithium ion batteries and that for this system the battery capacity would need to be 6.8 times higher than the supercapacitors one, to meet the imposed requirements, the supercapacitors present themselves as the more economically viable option. On top of that, the supercapacitors life span vastly exceeds the one of batteries which means that a battery implementation would require several replacements while the supercapacitors could still operate. The only drawback of the capacitor solution would be the added weight since this technology is about eight times heavier, per kWh, than its lithium ion alternative. Despite this drawback, given the massive difference in necessary capacity, the overall weight of a supercapacitor solution would only be around 20% heavier than a battery based one and all the supercapacitor advantages make it a clear favourite for this application.

Capacitors and supercapacitors have their capacity measured in Farad instead of kWh. To determine the number of capacitors required for this system, it is possible to calculate the energy stored by a capacitor and then, through equation 5.3, obtain its capacity in kWh.

$$E = \frac{1}{2} \cdot C \cdot V^2 \quad (5.6)$$

The most adequate capacitors currently available on the market have a capacity of 4000 Farad and an operating voltage of 4.2V. Applying these values to equation 5.6 it becomes,

$$E = \frac{1}{2} \cdot 4000 \cdot 4.2^2 = 35280J \quad (5.7)$$

$$C = \frac{35280}{3600 \cdot 10^3} = 9.8Wh \quad (5.8)$$

From this it is possible to determine that there will be required 15788 supercapacitors with the specified characteristics. With some calculations and with a set voltage of 700V for the OESS (a standard value for energy storage devices), it is possible to determine that the ideal layout for the supercapacitors is 94 parallel strings of 168 supercapacitors each. This configuration requires 15792 supercapacitors (only four more than the ideal number) and the voltage of the storage device is 705.6V.

5.3 Matlab implementation

To implement the capacitor bank in Matlab/Simulink, the equivalent capacitance of the proposed capacitor configuration must be determined. This can be done by first calculating the capacitance of each parallel string of capacitors, followed by the calculation of the equivalent capacitance of the parallel of all the strings.

The equivalent capacitance of a series of capacitors is given as presented in the next equation:

$$C_{series} = \frac{1}{\frac{1}{C_1} + \frac{1}{C_2} + \frac{1}{C_3} + \dots + \frac{1}{C_n}} \quad (5.9)$$

Given that all the capacitors used for the OESS have an equal capacitance value, the expression above can be simplified as:

$$C_{series} = \frac{1}{\frac{n}{C}} \quad (5.10)$$

Replacing the variables in equation 5.10 for their values, it is obtained:

$$C_{series} = \frac{1}{\frac{168}{4000}} = 23.8095F \quad (5.11)$$

To calculate the total equivalent capacitance of the capacitor bank of all the 94 parallel capacitor strings, the following expression is used:

$$C_{parallel} = C_1 + C_2 + C_3 + \dots + C_n = n \cdot C \quad (5.12)$$

Solving equation 5.12 with its respective values it becomes:

$$C_{parallel} = 94 \cdot 23.8095 = 2238.0952F \quad (5.13)$$

5.4 DC/DC converter

As mentioned in 2.5.2, the charge/discharge converter will behave as a buck converter when the OESS is being charged and as a boost converter when it is being discharge and supplying power

to the DC link.

For the charging process, the boost converter can be described by the equations already discussed in 4.3. From equation 4.2, the expected duty-cycle of the transistor can be calculated.

$$D = 1 - \frac{705.6}{2200} = 0.679 \quad (5.14)$$

When the OESS is charging, and the converter works as a buck one, its transfer function is given as a relation with the transistors duty-cycle and can be described as follows.

$$\frac{V_o}{V_{in}} = D \quad (5.15)$$

While operating in charging mode, it is expected the duty-cycle of the transistor to be:

$$D = \frac{705.6}{2200} = 0.3207 \quad (5.16)$$

5.5 DC/DC converter control

5.5.1 Charging OESS

When the train is braking by means of the electric motors, the regenerated power is sent to the DC link capacitor and, if it is not sent elsewhere, the voltage of the DC link capacitor will increase indefinitely, destroying this capacitor and disabling the train. To send the power from the DC link to the OESS while guarantying that the traction system maintains its correct operation, a controller for the transistor was implemented.

This controller is activated when the speed controller enters the braking mode. The reference charging current, is subtracted to the measured charging current to obtain an error value. This error is then divided by the reference value of this current to normalize the signal. From this, a PI controller is used to process the error signal and outputs a reference duty-cycle value for the PWM generator block, whose pulses will be used to driver the transistor one.

This controller's implementation in the Matlab/Simulink environment can be further analysed in figure 5.1

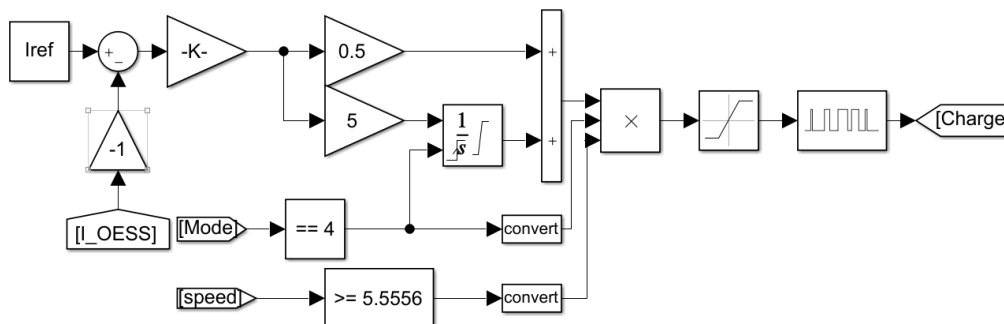


Figure 5.1: DC/DC bidirectional converter charge controller

5.5.2 Discharging OESS

The charge stored in the OESS will be used to reduce the power required from the catenary during acceleration events. To create the controller, first it is necessary to estimate the available power that is recovered from braking events. If energy recovered is considered to be 75% of the kinetic energy, with the remaining 25% being wasted due to drag forces, the recovered energy amounts to 116.04kWh.

Knowing that the train takes around 200 seconds to achieve its maximum speed, this means that throughout this time the OESS will have, on average, an available power of:

$$P_{avg} = \frac{116.04 \cdot 3600}{200} = 2088.72kW \quad (5.17)$$

From this average output power, the output current of the battery can be determined by:

$$I = \frac{P}{V} = \frac{2088.72k}{705.6} = 2960.20A \quad (5.18)$$

Since the power consumed by the train is small at low speeds, the OESS is only used when the train is accelerating at a velocity higher than half the synchronism velocity, 9.5238m/s. The remain of the controller is a standard PI controller where the error of the discharge current is used for the PI controller to generate a duty-cycle reference for the PWM signal, that drives the transistor. The controller's implementation in Matlab/Simulink's environment can be seen below.

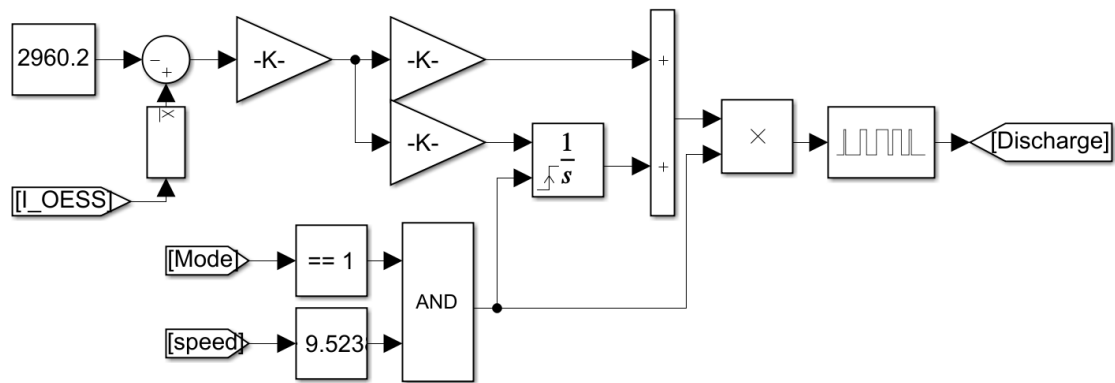


Figure 5.2: DC/DC bidirectional converter discharge controller

Chapter 6

Results

6.1 Photovoltaic Production System

To test the photovoltaic system implemented in the simulation environment of Matlab/Simulink, three tests were done to evaluate the performance of the system. At first, the auxiliary system was tested without the photovoltaic production system connected, and the current that passed through the coil was measured and its RMS value was integrated. The result is shown in the image below.

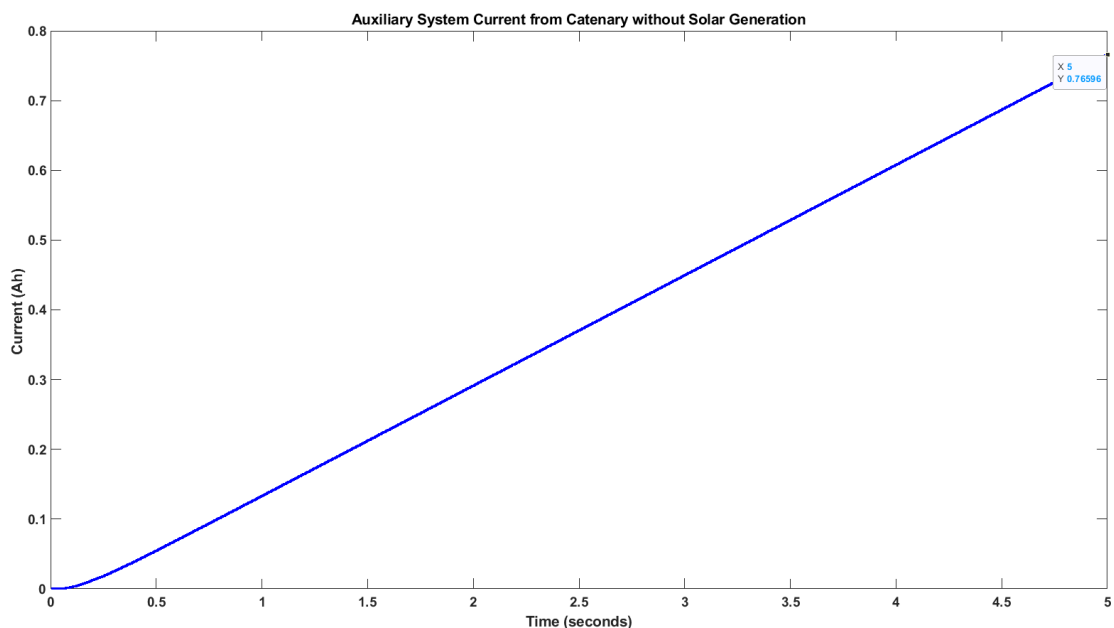


Figure 6.1: Current consumed by the auxiliary systems without photovoltaic system connected

From this test it was measured that the catenary supplied the auxiliary systems with a current of 0.76596Ah over the period of five seconds in which the catenary was the only power source for the auxiliary systems.

For the second simulation, the photovoltaic production systems was connected to the DC link of the auxiliary systems and to test the stability of the controller, the irradiance level provided to the solar panel block was a step, at 0.1s, with an amplitude of 1000. This means that for this test the solar panels start in a pitch black environment and at the instant 0.1s the irradiance level on their surface varies instantly to 1000W/m^2 . The results that follow present the current supplied by the catenary to the auxiliary systems over the course of five seconds, while the solar panels work at their nominal power. The voltage, current and power outputted by an array of 90 solar panels, corresponding to the BBS and BBN carriages, is also presented.

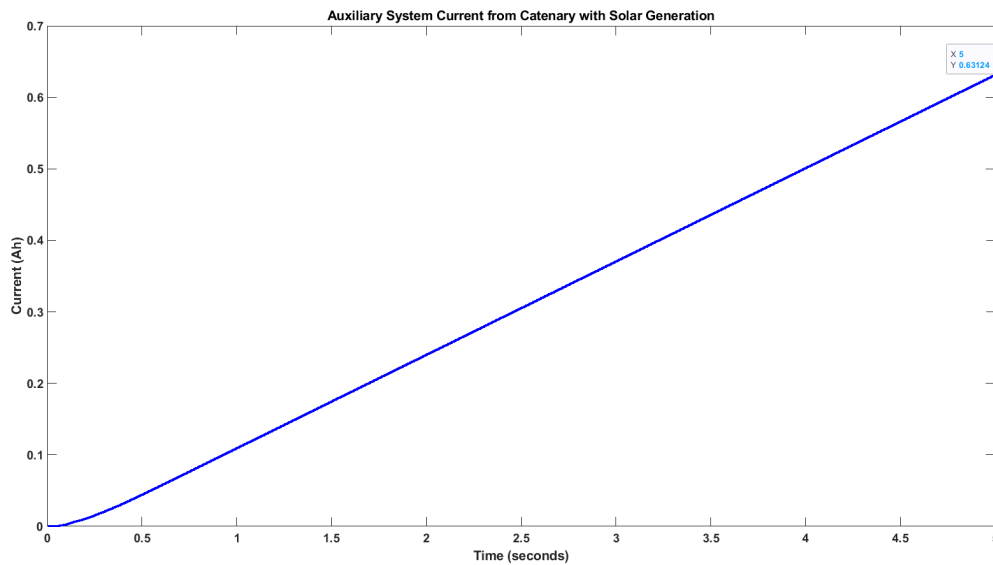


Figure 6.2: Current consumed by the auxiliary systems with photovoltaic system connected with nominal irradiance

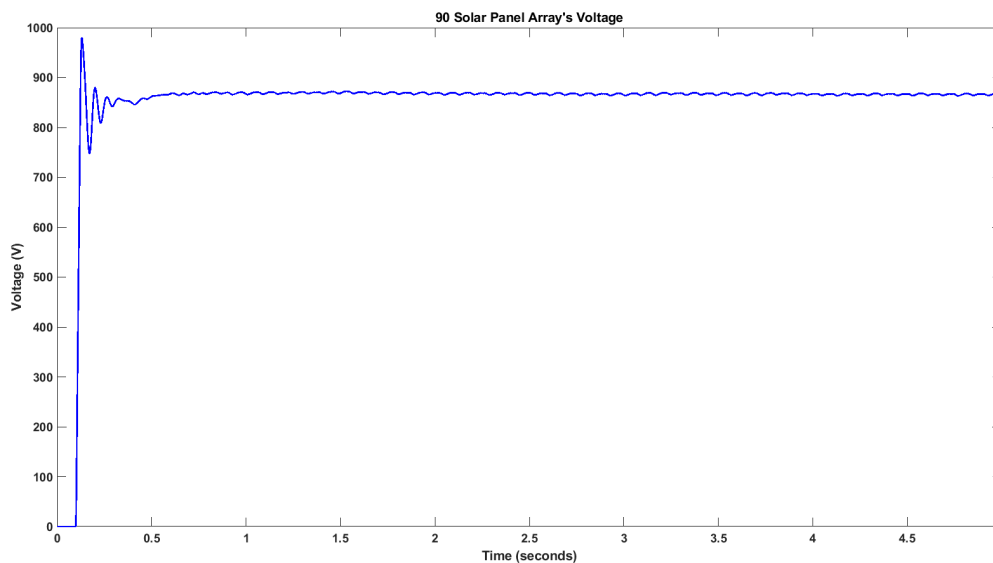


Figure 6.3: Voltage at the output of an array of 90 solar panels

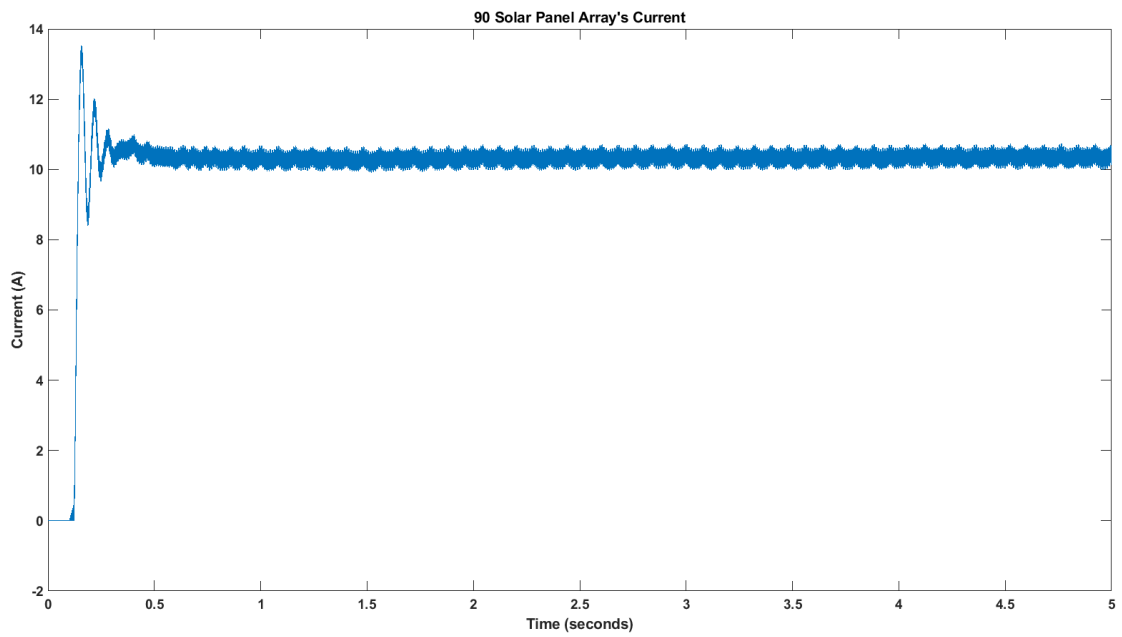


Figure 6.4: Current at the output of an array of 90 solar panels

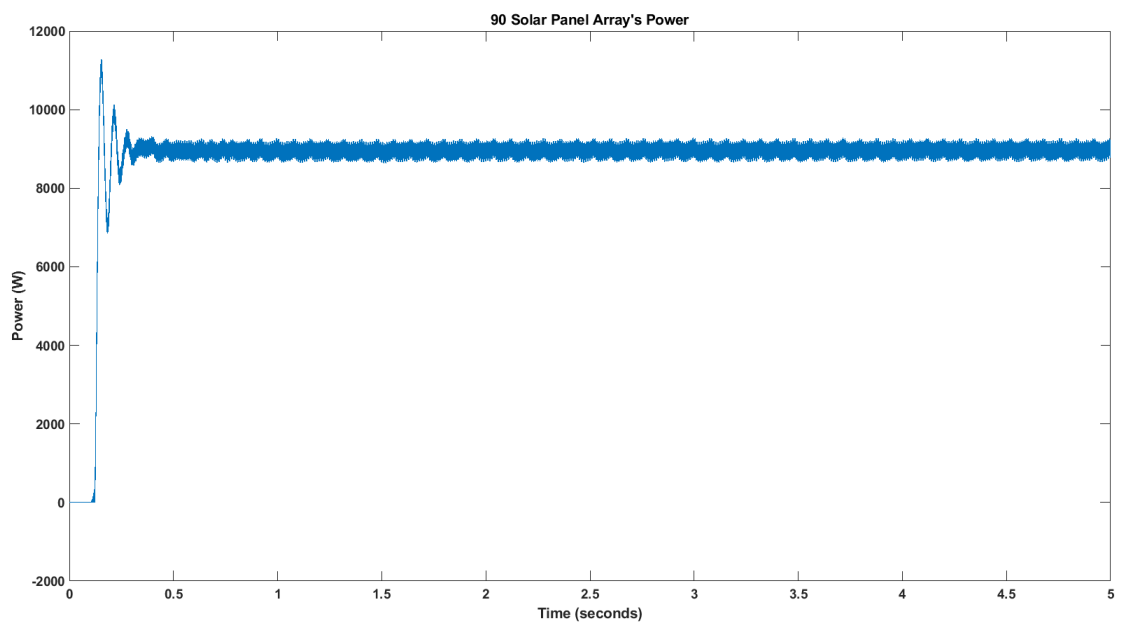


Figure 6.5: Power outputted by an array of 90 solar panels

From figure 6.2 it is possible to conclude that the photovoltaic production has an effective positive impact on the auxiliary systems power requirements from the catenary since for the same period, the current from the catenary reduced from 0.76596Ah to 0.63124Ah.

The figures that display the voltage, current and power from the output of the array of 90 solar

panels also shows that the controller implemented to achieve the best efficiency possible for the solar production is working as intended since the panels produce 9kW of power. It is also possible to notice in the figure displaying the voltage of the array, the corrections done by the controller to maximize the power output at 0.5 seconds.

The sky, unlike what was considered in the previous test, is not always clear and many times there is the interference of clouds, that lead to a drop in the irradiance levels. To test the ability of the MPPT controller to extract the maximum amount of power possible out of the solar panels in this situations a third test was designed where the panels began with an irradiance value of 1000 and at the instant 1 second, the irradiance level drops in a step to 750. This variation is intended to simulate a cloud passing in front of the sun. The results obtained for this tests are shown below with the same signals as the previous test.

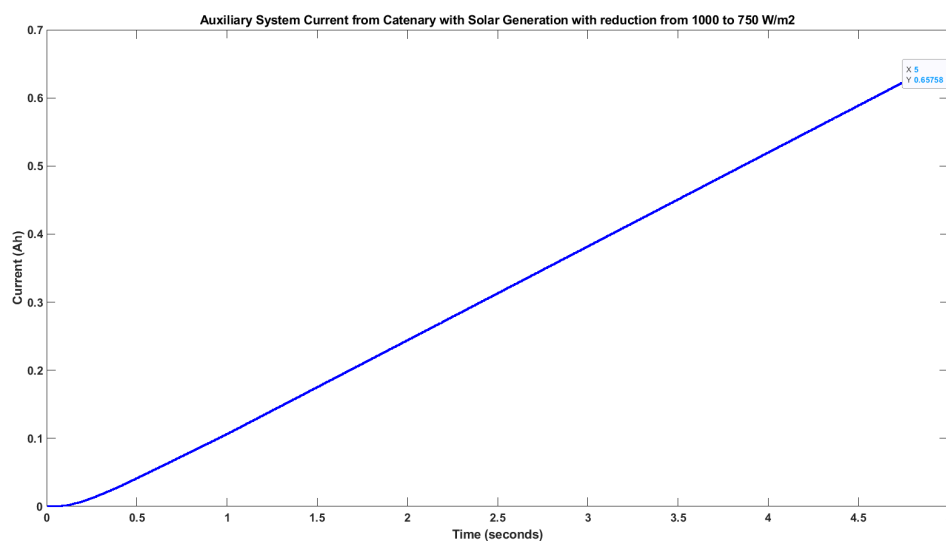


Figure 6.6: Current consumed by the auxiliary systems with photovoltaic system connected with an irradiance variation from 1000 to 750 W/m²

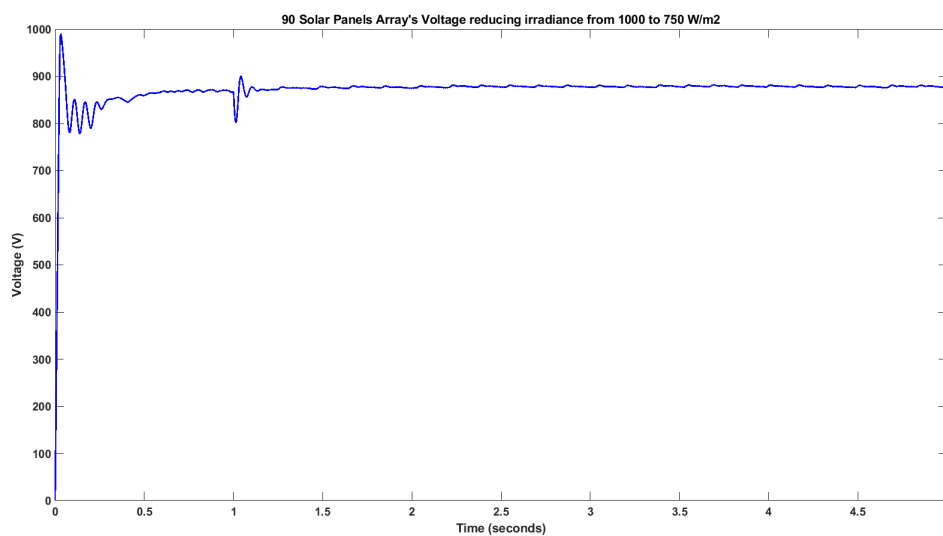


Figure 6.7: Voltage at the output of an array of 90 solar panels with an irradiance variation from 1000 to 750 W/m²

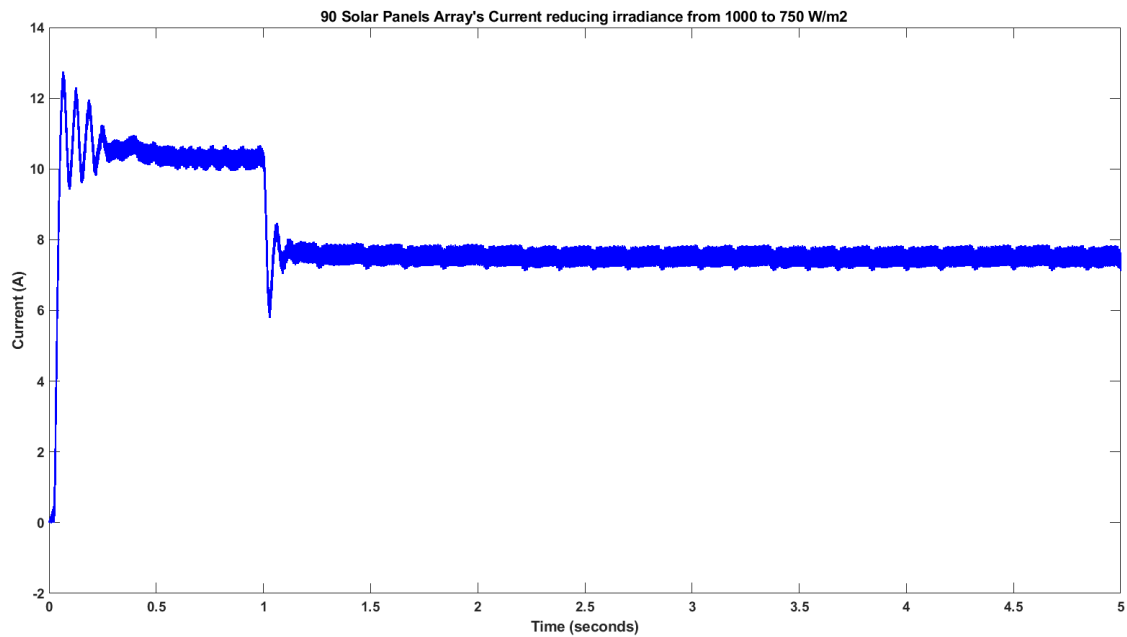


Figure 6.8: Current at the output of an array of 90 solar panels with an irradiance variation from 1000 to 750 W/m²

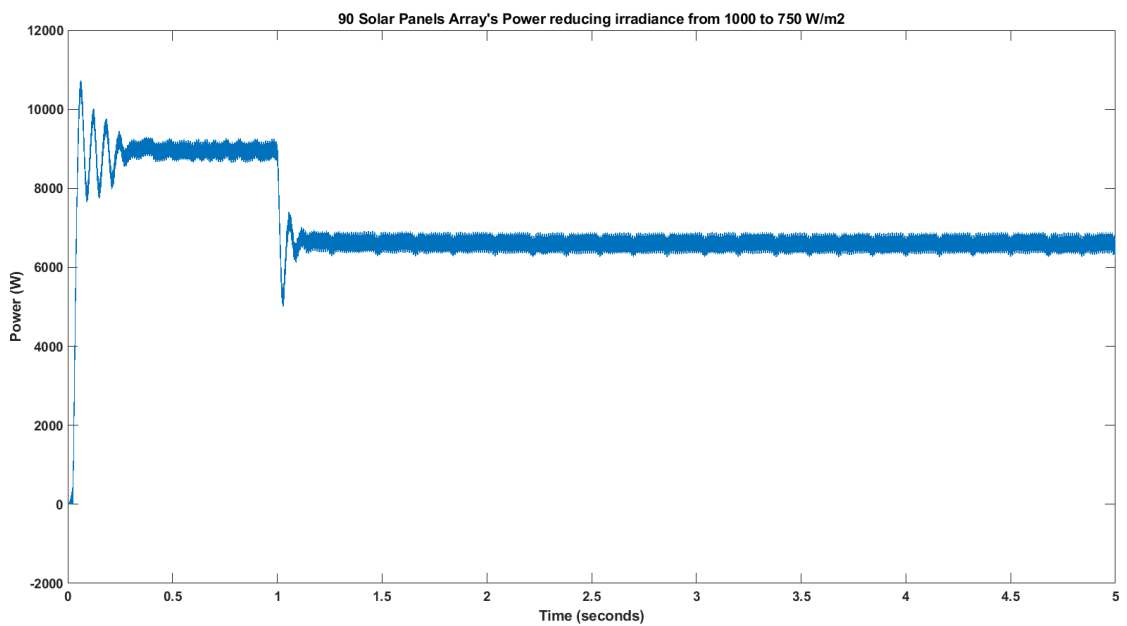


Figure 6.9: Power outputted by an array of 90 solar panels with an irradiance variation from 1000 to 750 W/m²

From figure 6.6 it can be concluded that the photovoltaic production system is still injecting the produced power correctly into the auxiliary system DC link since the current measured entering

the system through via the catenary is still lower than the one measured in the first test, with this being 0.65758Ah. It is also to note that the current measured in this test is higher than the one measured in the previous one, as it was expected because the available power to be generated is lower.

6.2 Onboard Energy Storage System

Due to the very large amount of data generated by the model implemented in Matlab/Simulink (dozens of Gigabytes per simulation), and the lack of computational power available to run this simulations, the traction system simulations were only done for speeds between zero and ninety kilometers per hour. Despite neglecting the higher speeds, this speed range captures both the constant torque and constant power modes of operation of the motors and provides good information regarding the power consumed by the train with and without an OESS.

The first simulation was done without any battery system and the power resulting from the electrical braking was dissipated as heat through banks of resistors. As mentioned this simulation covers the speed range between 0 and 90 km/h and it consists in accelerating from a standstill to 90km/h, maintaining that speed for a few seconds and then braking until the train stops.

The following images show the velocity curve done by the train in this test, the torque evolution across the different driving modes and the charge consumed from the catenary by the traction system, respectively.

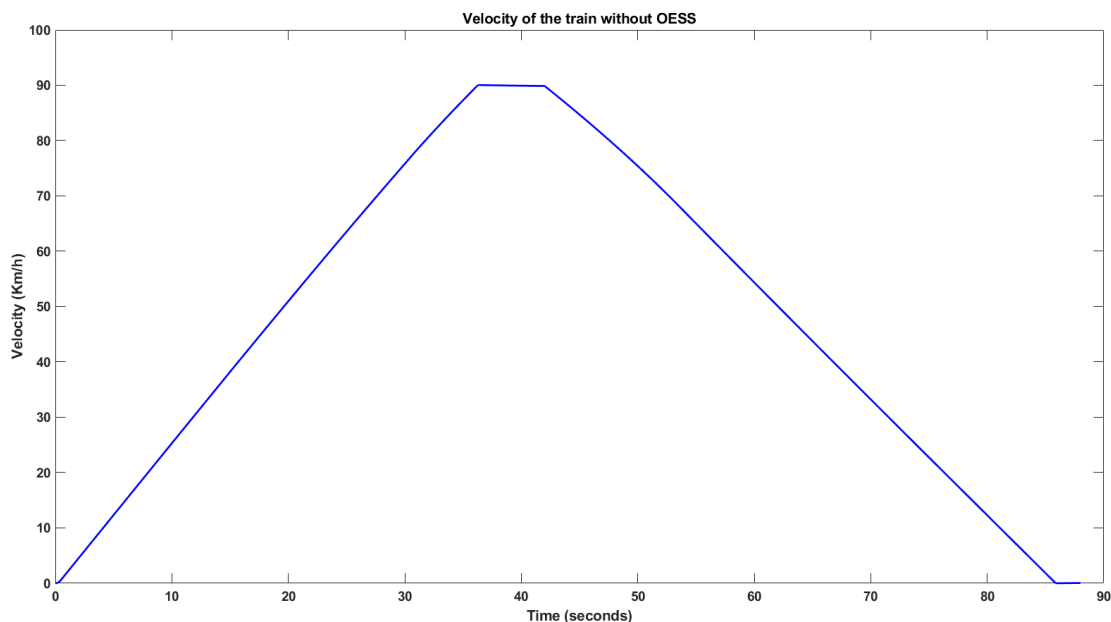


Figure 6.10: Velocity of the train during acceleration and deceleration test without OESS

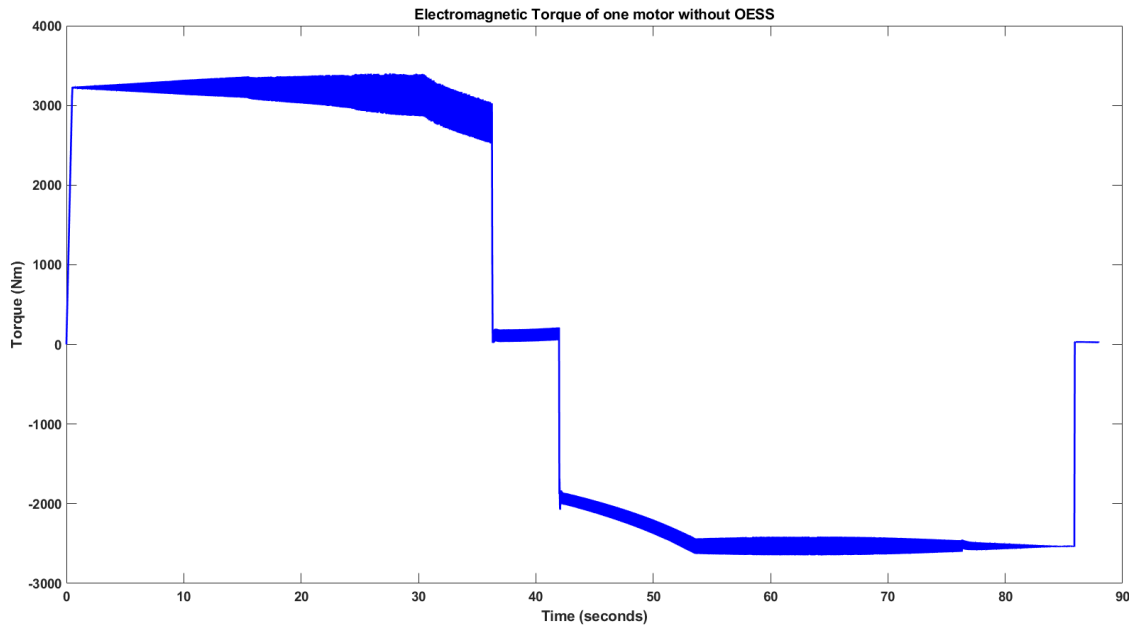


Figure 6.11: Torque of one of the motors of the train during acceleration and deceleration test without OESS

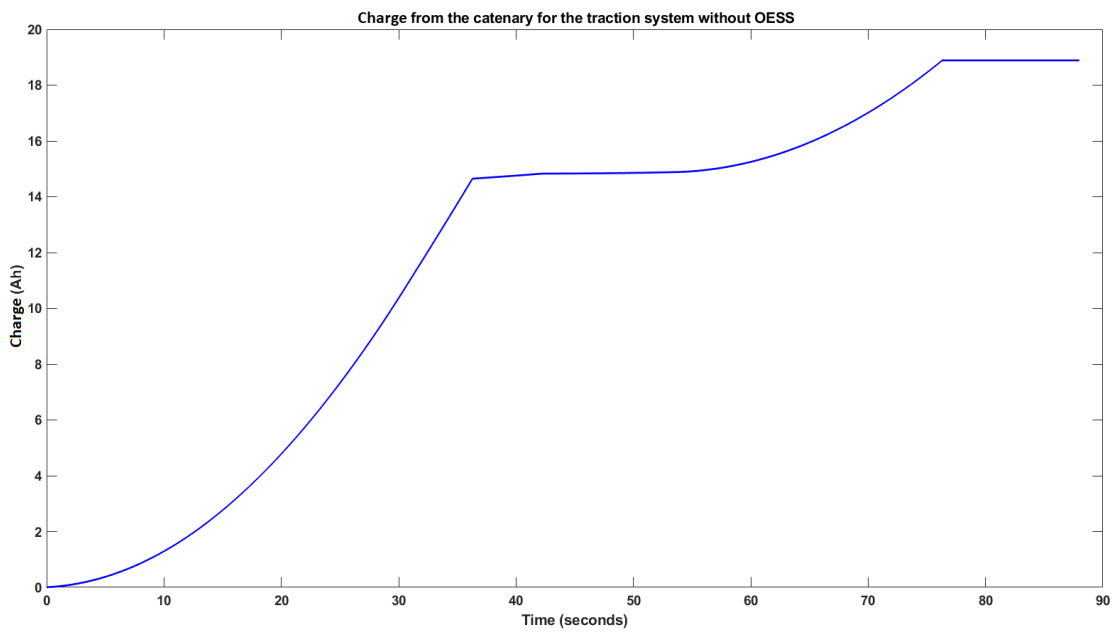


Figure 6.12: Charge consumed from the catenary by the traction system of the train during acceleration and deceleration test without OESS

From the first figure it is possible to note the impact that the air drag has at high speeds. On the C codes developed in subsection 3.2, the train took 40 seconds more to accelerate than to brake and for the lower velocities of this simulation, due to the reduced air drag, the train accelerates faster than it brakes. From the figure that displays the motor's torque it is possible to observe in action the controllers implemented to manage the different operating modes:

- 0-30 seconds acceleration without field weakening
- 30-36 seconds acceleration with field weakening
- 36-42 seconds cruising
- 42-56 seconds braking with field weakening
- 56-86 seconds braking without field weakening
- 86-... seconds train remains still

From this figure it is also possible to view that the torque of the motor as a significant ripple due to both the controller and the parameterization of the motor.

From the third image it can be taken that the traction system, during the 90 seconds that the train was moving, consumed 19Ah. The different operation modes can be noticed in the variations of this curve.

For the second test of this system, the OESS was fitted to the traction system and the same test was repeated. The images bellow show the results obtain in the same order as in the previous test.

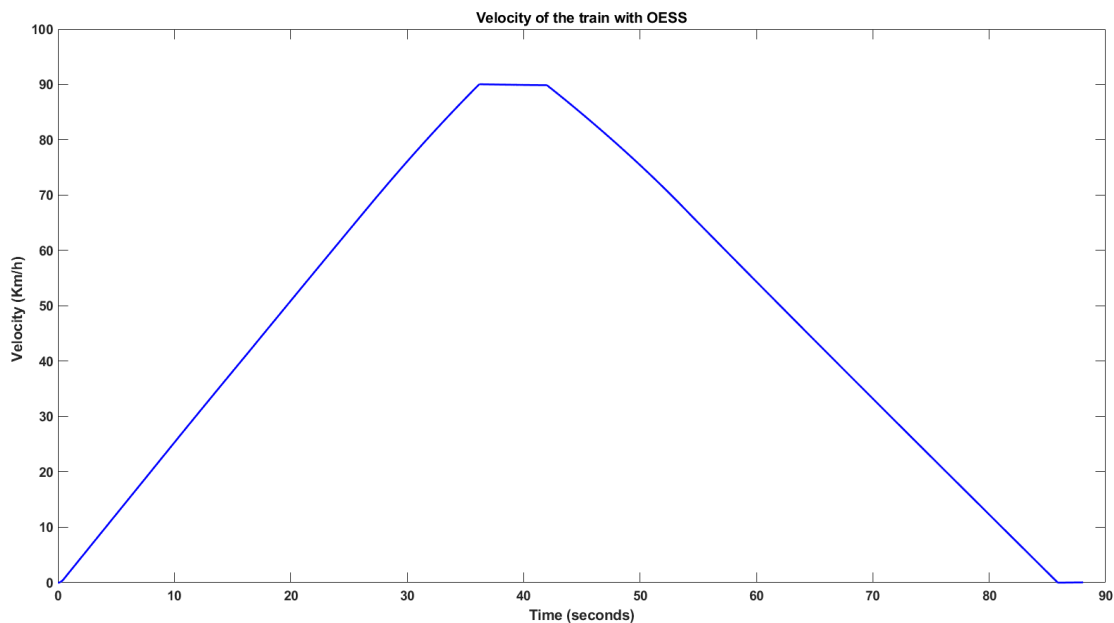


Figure 6.13: Velocity of the train during acceleration and deceleration test with OESS

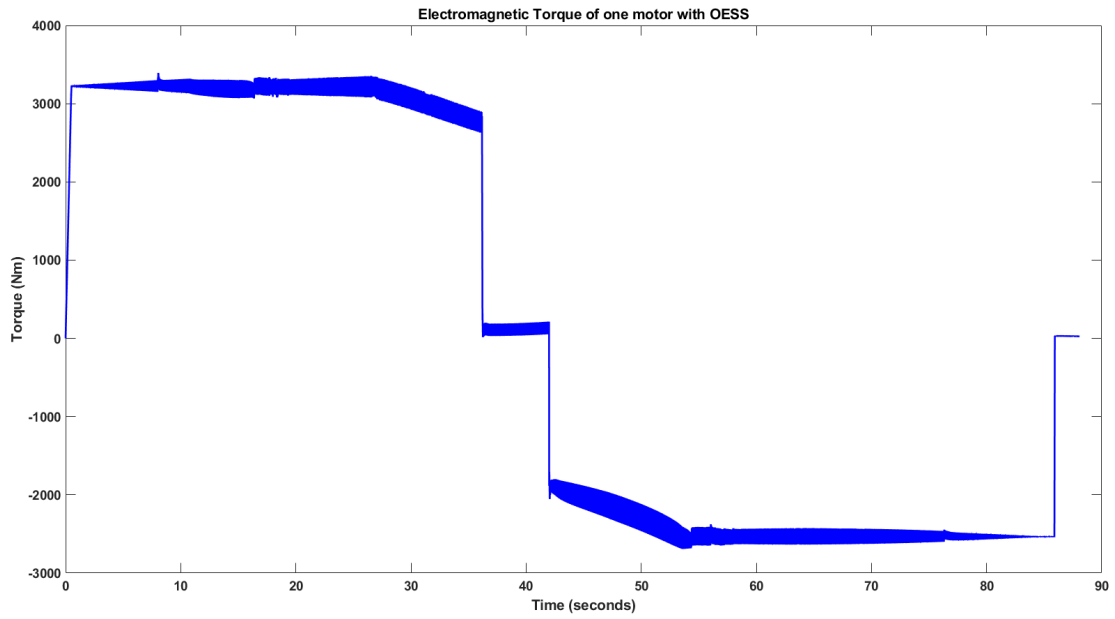


Figure 6.14: Torque of one of the motors of the train during acceleration and deceleration test with OESS

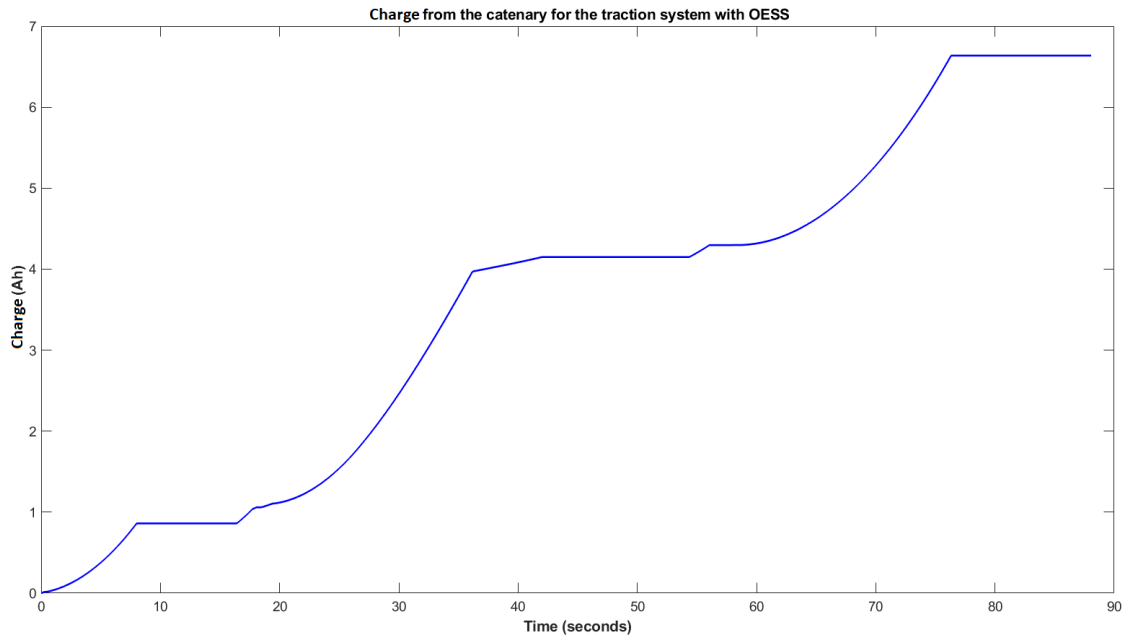


Figure 6.15: Charge consumed from the catenary by the traction system of the train during acceleration and deceleration test with OESS

The figures showing the velocity and torque of this test, with OESS implemented, can be compared to the ones of the previous test, without OESS, so that it can be concluded that the effort made by the traction system in both tests is the same. On the figures that includes the torque of the motors, It is noticeable that the ripple is slightly different between them, due to the controller not being 100% optimal, but the average value of the torque is equal for both of the tests.

Knowing this, the results that presents the charge consumed by the traction system from the catenary in both tests can be compared and the improvement obtained with the OESS installed is very significant. With the OESS installed in the train, the consumption was 2.8 times lower than the one without the OESS. This means that the regenerative braking was able to recover almost two thirds of the energy used during the acceleration process.

For last, the voltage of the capacitor bank was measured during the test with the storage system and the result is visible bellow.

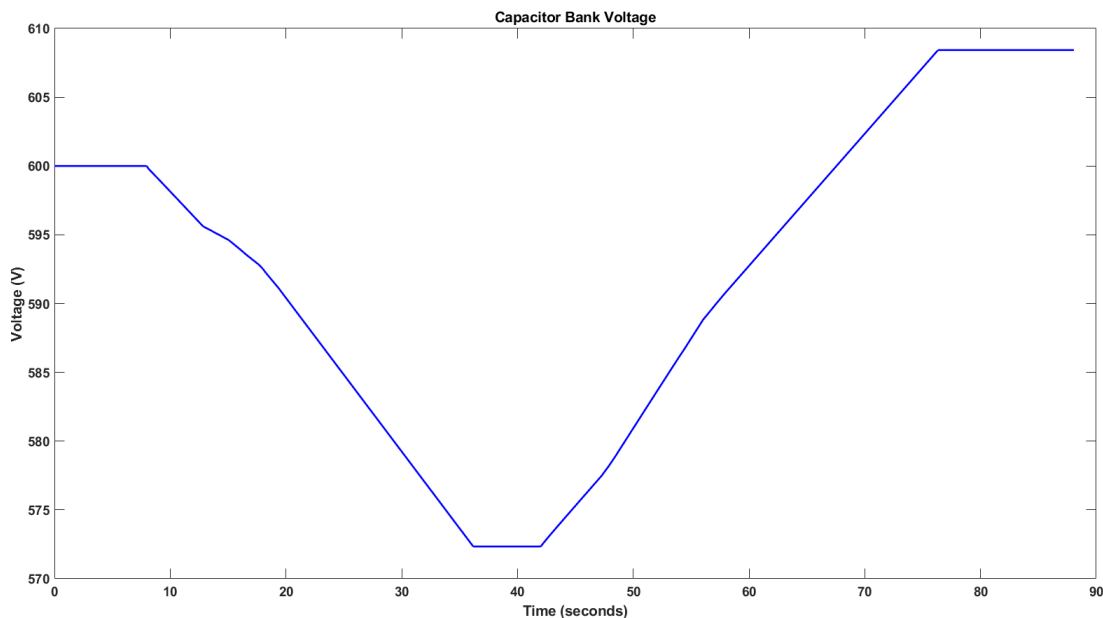


Figure 6.16: Voltage of the capacitor bank of the train during acceleration and deceleration test with OESS

From this graph it is possible to conclude that the current used to charge the battery surpassed the one used from the battery to power the train. This means that with a more elaborate control method, the energy savings can still be considerably improved.

Chapter 7

Conclusion

7.1 Final Remarks

Through the course of the development of this dissertation, many different systems had to be studied and analysed in order to proceed to their implementation. The large number of components led to the implementation of some of them to not achieve an optimum level but, in the end, all of them fulfilled their purpose. The auxiliary systems inverter was able to generate a three phase balanced sinusoidal grid to feed all the required components and when work was built upon this system it worked as intended.

The photovoltaic generation system was able to accomplish its goal and generate a significant amount of power that contributes for the reduction in grid power consumption and the controller is able to maintain peak efficiency for different irradiance levels.

Regarding the traction system, it is able to simulate the movement of the train across its speed range with a great degree of accuracy. Even though the ripple is larger than it is desired, that fact did not induce any significant problems.

The battery charge and discharge systems, even being very simple proved to have an enormous impact on the overall efficiency of the train when it is performing velocity variations. The storage system is even capable of sustaining the train's operation on its own, in case of a power outage or during a period when the catenary is suppressed to change the catenary that feeds the train, because of the use of supercapacitors that are able to achieve very large power deliveries.

7.2 Future Work

Due to the vast number of controllers that were required to be implemented during the development of this dissertation, their optimization was not always as good as it would be desired. In the future the optimization of the train's traction controller could make a significant difference in the train stability and the high ripples that can be observed in many signals, especially in the torque.

The battery controllers optimization could lead to significant power savings, mainly the reference currents should be generated by a controller instead of being constant, to reflect the variations

in regenerated power that occur during the train's accelerations and decelerations. This would consist on the implementation of a battery management system.

Besides the controllers, the implementation of a small scale system could be extremely useful to validate the simulation work. This experimental work could also be used to study some physical components with more detail, like the motor, to obtain a better characterisation of its parameters and a more accurate model.

Appendix A

C Code

A.1 Code used to calculate the acceleration time of the train

```
1  #include <stdio.h>
2
3  √ float accel(float vant, float vsync){
4
5      if(vant <= vsync) return (210000-(2000+40*vant+6.9*vant*vant))/298300;
6      else return (4000000/298300/vant)-(2000+40*vant+6.9*vant*vant)/298300;
7
8  }
9
10 √ int main(){
11
12     float passo = 10, vmax = 220/3.6, v = 0/3.6, vant = v, vsync = 19.0476;
13     int i = 0;
14
15     √ for(i = 1; v < vmax; i++){
16         v = vant + accel(vant, vsync) * passo;
17         vant = v;
18         printf("Tempo: %.4f, Velocidade %.4f\n", i*passo, v);
19     }
20 }
21
```

Figure A.1: Code used to calculate the acceleration time of the train

A.2 Code used to calculate the deceleration time of the train

```
1  #include <stdio.h>
2
3  float accel(float vant, float vsync){
4
5      if(vant <= vsync) return (210000-(2000+40*vant+6.9*vant*vant))/298300;
6      else return (4000000/298300/vant)-(2000+40*vant+6.9*vant*vant)/298300;
7
8  }
9
10 int main(){
11
12     float passo = 10, vmax = 220/3.6, v = 0/3.6, vant = v, vsync = 19.0476;
13     int i = 0;
14
15     for(i = 1; v < vmax; i++){
16         v = vant + accel(vant, vsync) * passo;
17         vant = v;
18         printf("Tempo: %.4f, Velocidade %.4f\n", i*passo, v);
19     }
20 }
21
```

Figure A.2: Code used to calculate the deceleration time of the train

Appendix B

Traction System

B.1 Torque Reference Controller

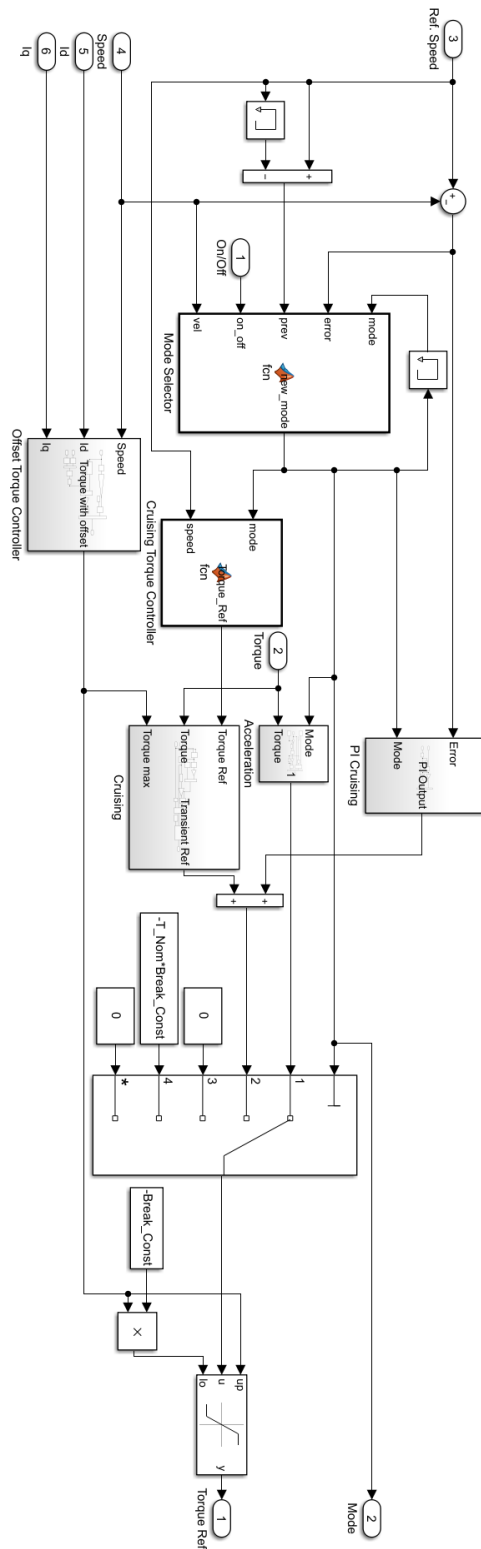


Figure B.1: Torque Reference Controller implementation in Matlab/Simulink

B.2 Electrical System

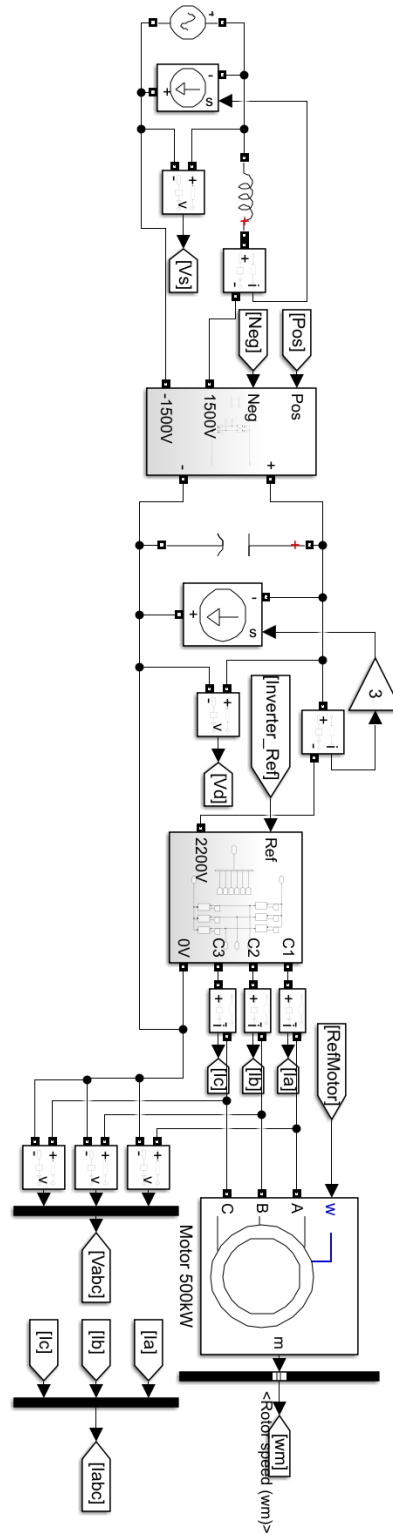


Figure B.2: Electrical model of the traction system implemented in Matlab/Simulink

Appendix C

Schematic

C.1 Series 4000 schematic

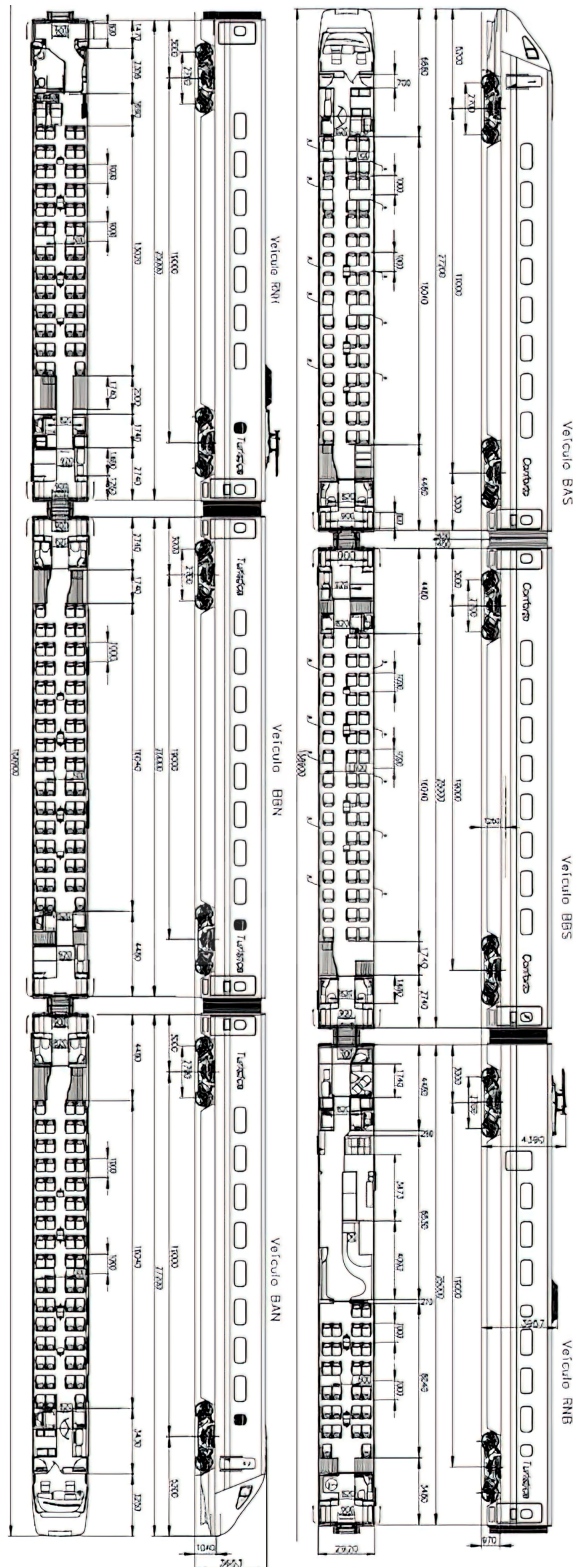


Figure C.1: Schematic of the series 4000 train from [3]

Appendix D

MPPT

D.1 MPPT implementation

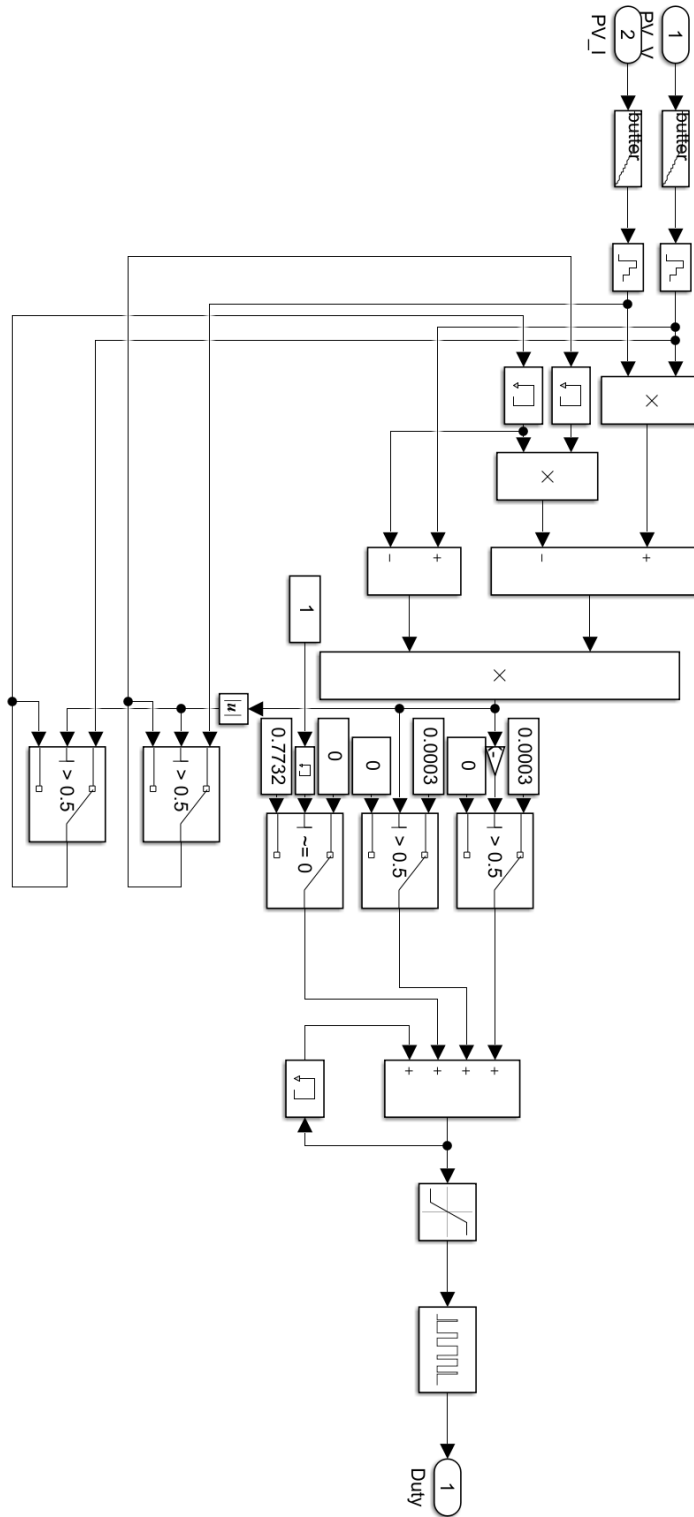


Figure D.1: MPPT algorithm implementation in Matlab/Simulink

References

- [1] H. Kumar, S. K. Yadav, K. Sahay, and S. S. Kumar. Investigation on recuperation of regenerative braking energy using ess in (urban) rail transit system. In *2019 International Conference on Electrical, Electronics and Computer Engineering (UPCON)*, pages 1–6, 2019. doi:10.1109/UPCON47278.2019.8980241.
- [2] Diogo Ribeiro, Rui Calçada, Raimundo Delgado, Maik Brehm, and Volkmar Zabel. Finite-element model calibration of a railway vehicle based on experimental modal parameters. *Vehicle System Dynamics*, 51, 06 2013. doi:10.1080/00423114.2013.778416.
- [3] Comboios de Portugal. Comboio série 4001-4010 e 4051-4060: Cp. accessed july. 29, 2021. URL: <https://www.cp.pt/institucional/pt/cultura-ferroviaria/frota-material-circulante/material-4001-4010-e-4051-4060>.
- [4] S. de la Torre, A. J. Sánchez-Racero, J. A. Aguado, M. Reyes, and O. Martínez. Optimal sizing of energy storage for regenerative braking in electric railway systems. *IEEE Transactions on Power Systems*, 30(3):1492–1500, 2015. doi:10.1109/TPWRS.2014.2340911.
- [5] Hannah Ritchie. Which form of transport has the smallest carbon footprint?. accessed july 29, 2021, Oct 2020. URL: <https://ourworldindata.org/travel-carbon-footprint>.
- [6] Ali Abdul and Razzaq Altahir. Park and clark transformations park and clark transformations: A short review. ., 2020. URL: <http://rgdoi.net/10.13140/RG.2.2.20287.46241>, doi:10.13140/RG.2.2.20287.46241.
- [7] Derya Ahmet Kocabas, Emrah Salman, and Ahmet Kubilay Atalay. Analysis using d-q transformation of a drive system including load and two identical induction motors. In *2011 IEEE International Electric Machines Drives Conference (IEMDC)*, pages 1575–1578, 2011. doi:10.1109/IEMDC.2011.5994596.
- [8] Shailendra Jain and Lalit Kumar. 31 - fundamentals of power electronics controlled electric propulsion. In Muhammad H. Rashid, editor, *Power Electronics Handbook (Fourth Edition)*, pages 1023–1065. Butterworth-Heinemann, fourth edition edition, 2018. URL: <https://www.sciencedirect.com/science/article/pii/B9780128114070000350>, doi:<https://doi.org/10.1016/B978-0-12-811407-0.00035-0>.
- [9] Richard Crowder. 7 - induction motors. In Richard Crowder, editor, *Electric Drives and Electromechanical Systems (Second Edition)*, pages 187–207. Butterworth-Heinemann, second edition edition, 2020. URL: <https://www.sciencedirect.com/science/article/pii/B9780081028841000078>, doi:<https://doi.org/10.1016/B978-0-08-102884-1.00007-8>.

- [10] Sang-Hoon Kim. Chapter 8 - high-speed operation of alternating current motors. In Sang-Hoon Kim, editor, *Electric Motor Control*, pages 341–371. Elsevier, 2017. URL: <https://www.sciencedirect.com/science/article/pii/B9780128121382000088>, doi:<https://doi.org/10.1016/B978-0-12-812138-2.00008-8>.
- [11] Cord-H Dustmann. Advances in zebra batteries. *Journal of Power Sources*, 127(1):85–92, 2004. Eighth Ulmer Electrochemische Tage. URL: <https://www.sciencedirect.com/science/article/pii/S0378775303009418>, doi: <https://doi.org/10.1016/j.jpowsour.2003.09.039>.
- [12] M.A. Fetcenko, S.R. Ovshinsky, B. Reichman, K. Young, C. Fierro, J. Koch, A. Zallen, W. Mays, and T. Ouchi. Recent advances in nimh battery technology. *Journal of Power Sources*, 165(2):544–551, 2007. IBA – HBC 2006. URL: <https://www.sciencedirect.com/science/article/pii/S0378775306021215>, doi: <https://doi.org/10.1016/j.jpowsour.2006.10.036>.
- [13] Tosaphol Ratniyomchai, Pietro Tricoli, and Stuart Hillmansen. Recent developments and applications of energy storage devices in electrified railways. *IET Electrical Systems in Transportation*, 4:9–20, 03 2014. doi:[10.1049/iet-est.2013.0031](https://doi.org/10.1049/iet-est.2013.0031).
- [14] Masataka Wakihara. Recent developments in lithium ion batteries. *Materials Science and Engineering: R: Reports*, 33(4):109–134, 2001. URL: <https://www.sciencedirect.com/science/article/pii/S0927796X01000304>, doi: [https://doi.org/10.1016/S0927-796X\(01\)00030-4](https://doi.org/10.1016/S0927-796X(01)00030-4).
- [15] Jie Sun, Jigang Li, Tian Zhou, Kai Yang, Shouping Wei, Na Tang, Nannan Dang, Hong Li, Xinping Qiu, and Liquan Chen. Toxicity, a serious concern of thermal runaway from commercial li-ion battery. *Nano Energy*, 27:313–319, 2016. URL: <https://www.sciencedirect.com/science/article/pii/S2211285516302130>, doi: <https://doi.org/10.1016/j.nanoen.2016.06.031>.
- [16] M. Khodaparastan, A. A. Mohamed, and W. Brandauer. Recuperation of regenerative braking energy in electric rail transit systems. *IEEE Transactions on Intelligent Transportation Systems*, 20(8):2831–2847, 2019. doi:[10.1109/TITS.2018.2886809](https://doi.org/10.1109/TITS.2018.2886809).
- [17] Jiří Libich, Josef Máca, Jiří Vondrák, Ondřej Čech, and Marie Sedlaříková. Supercapacitors: Properties and applications. *Journal of Energy Storage*, 17:224–227, 2018. URL: <https://www.sciencedirect.com/science/article/pii/S2352152X18301634>, doi: <https://doi.org/10.1016/j.est.2018.03.012>.
- [18] Ko, Park, and Lee. Regenerative battery charging control method for pmsm drive without a dc/dc converter. *Electronics*, 8:1126, 10 2019. doi:[10.3390/electronics8101126](https://doi.org/10.3390/electronics8101126).
- [19] Nadarajah Kannan and Divagar Vakeesan. Solar energy for future world: - a review. *Renewable and Sustainable Energy Reviews*, 62:1092–1105, 2016. URL: <https://www.sciencedirect.com/science/article/pii/S1364032116301320>, doi: <https://doi.org/10.1016/j.rser.2016.05.022>.
- [20] M. F. Nayan, S. M. S. Ullah, and S. N. Saif. Comparative analysis of pv module efficiency for different types of silicon materials considering the effects of environmental parameters. In *2016 3rd International Conference on Electrical Engineering and Information Communication Technology (ICEEICT)*, pages 1–6, 2016. doi:[10.1109/CEEICT.2016.7873089](https://doi.org/10.1109/CEEICT.2016.7873089).

- [21] Francesco Calise, Massimo Dentice D'Accadia, Massimo Santarelli, Andrea Lanzini, and Domenico Ferrero. *Solar Hydrogen Production*. Academic Press, 2019. URL: <https://www.sciencedirect.com/science/article/pii/B978012814853209994X>, doi:<https://doi.org/10.1016/B978-0-12-814853-2.09994-X>.
- [22] Russell H. Plante. *Solar Energy, Photovoltaics, and Domestic Hot Water*. Academic Press, Boston, 2014. URL: <https://www.sciencedirect.com/science/article/pii/B9780124201552160013>, doi:<https://doi.org/10.1016/B978-0-12-420155-2.16001-3>.
- [23] Piotr Lukaszewicz. *Energy Consumption and Running Time for Trains : modelling of running resistance and driver behaviour based on full scale testing*. PhD thesis, KTH, Vehicle Engineering, 2001. QC 20100526 NR 20140805.
- [24] W.J. Davis and General Electric Review. *The Tractive Resistance of Electric Locomotives and Cars*. General Electric, 1926. URL: <https://books.google.pt/books?id=hXkeHAAACAAJ>.
- [25] Agostinho Rocha, Armando Araújo, Adriano Carvalho, and João Sepulveda. A new approach for real time train energy efficiency optimization. *Energies*, 11(10):2660, October 2018. URL: <https://doi.org/10.3390/en11102660>, doi:10.3390/en11102660.
- [26] Lúgia Tatiana Duarte Monteiro. Análise da estabilidade de comboios em pontes ferroviárias sob ação de ventos laterais. Master's thesis, FEUP - Faculdade de Engenharia da Universidade do Porto, 6 2017.
- [27] Carlos Sicre, Asunción Cucala, Antonio Fernández, and Piotr Lukaszewicz. Modeling and optimizing energy-efficient manual driving on high-speed lines. *IEEE Transactions on Electrical and Electronic Engineering*, 7, 11 2012. doi:10.1002/tee.21782.
- [28] Train Logistic. Série 4000 - ficha técnica. accessed july 29, 2021. URL: https://www.trainlogistic.com/pt/Comboios/Gabinete/fich_atm4000.htm.
- [29] Li Changxian, Sun Yannan, and Li Chunying. Construction and simulation on traction converter and control system of emu. *Procedia Engineering*, 29:2980–2984, 2012. 2012 International Workshop on Information and Electronics Engineering. URL: <https://www.sciencedirect.com/science/article/pii/S1877705812004353>, doi:<https://doi.org/10.1016/j.proeng.2012.01.425>.
- [30] 100 watt 12 volt flexible monocrystalline solar panel. accessed july 29, 2021. URL: <https://www.renogy.com/100-watt-12-volt-flexible-monocrystalline-solar-panel/>.